Dnmt3aa But Not Dnmt3ab Is Required for Maintenance of Gametogenesis in Nile Tilapia

Feilong Wang
Southwest University
Zuliang Qin
Southwest University
Zhiqiang Li
Southwest University
Shuangyi Yang
Southwest University
Tian Gao
Southwest University
Lina Sun (sunlina@swu.edu.cn)
Southwest University https://orcid.org/0000-0002-6082-9473
Deshou Wang
Southwest University

Research

Keywords: Nile tilapia, DNA methylation, Dnmt3a, Gonad development, gametogenesis

Posted Date: August 12th, 2021

DOI: https://doi.org/10.21203/rs.3.rs-779232/v1

Dnmt3aa but not dnmt3ab is required for maintenance of gametogenesis in Nile tilapia

Feilong Wang†, Zuliang Qin†, Zhiqiang Li, Shuangyi Yang, Tian Gao, Lina Sun *

and Deshou Wang *

Key Laboratory of Freshwater Fish Reproduction and Development (Ministry of Education), Key Laboratory of Aquatic Science of Chongqing, School of Life Sciences, Southwest University, 400715, Chongqing, P.R. China.

* Correspondence: sunlina@swu.edu.cn; wdeshou@swu.edu.cn.

† These authors contributed equally to this work.

Abstract

Background: *Dnmt3a*, a *de novo* methylatransferase, is essential for both male and female germ line DNA methylation. Only one *Dnmt3a* is identified in mammals, and homozygous mutation of *Dnmt3a* is lethal, while two *Dnmt3a*, *dnmt3aa* and *dnmt3ab*, are identified in teleosts due to the third round of genome duplication, and homozygous mutation of *dnmt3aa* and *dnmt3ab* is viable in zebrafish. *Dnmt3aa* and *dnmt3ab* were demonstrated to have essential and non-overlapped functions on modulating behavioral control, however, their function in gonadal development is unclear in fish.

Results: In this study, the expression patterns of *dnmt3aa* and *dnmt3ab* in developing gonads of Nile tilapia was analyzed by quantitative real time PCR and fluorescence *in situ* hybridization. Both *dnmt3aa* and *dnmt3ab* displayed sexually dimorphic expression in developing gonads. *Dnmt3aa* was widely expressed in gonadal germ cells and somatic cells, highly expressed in oogonia, phase I and II oocytes and granulosa cells in ovaries and spermatogonia and spermatocytes in testes, while *dnmt3ab* was mainly expressed in ovarian granulosa cells and

testicular spermatocytes. Mutation of *dnmt3aa* and *dnmt3ab* was achieved by CRISPR/Cas9 in tilapia. Lower GSI (Gonadosomatic index), increased apoptosis of oocytes and spermatocytes and significantly reduced sperm quality were observed in $dnmt3aa^{-/-}$ mutants, while no obvious phenotype was observed in $dnmt3ab^{-/-}$ mutants. Consistently, the expression of apoptotic genes was significantly increased in $dnmt3aa^{-/-}$ mutants. In addition, *dnmt3aa* and *dnmt3ab* were found to have certain compensatory effects in the gonads. The global DNA methylation level in ovaries and testes of $dnmt3aa^{-/-}$ mutants was decreased significantly, compared with that of $dnmt3ab^{-/-}$ mutants and WT.

Conclusions: Taken together, our results suggest that *dnmt3aa*, not *dnmt3ab*, plays important roles in maintaining gametogenesis in teleost. Our results enrich the understanding of the function of DNA methyltransferases in gonads of non-mammalian vertebrates.

Keywords: Nile tilapia; DNA methylation; Dnmt3a; Gonad development; gametogenesis.

Background

DNA methylation, a mechanism of epigenetics plays crucial role in the control of development related gene expression during gametogenesis and early embryogenesis [1, 2]. During germ cells development, epigenetic reprogramming occurs dynamically, remodeling of DNA methylation marks in particular [3, 4]. At day 7.5 of early embryo (E7.5) in mouse, global DNA methylation of primordial germ cells (PGCs) is erased. Later, *De novo* DNA methylation proceeds differentially between male and female germ cells, earlier in spermatogenesis than in oogenesis. In the female germ cells, *de novo* DNA methylation occurs in arrested oocytes in meiotic prophase I. However, in the male germ cells, it takes place in mitotically arrested prespermatogonia before birth [5-7].

DNA methylation is catalyzed by a group of enzymes called DNA methyltransferases (*dnmts*), including *Dnmt1* and *Dnmt3*. *Dnmt1* is involved in the methylation of hemimethylated DNA and thus called maintenance DNA methyltransferase, while *Dnmt3* is able to place methylation marks on previously unmethylated CpGs of DNA and thus mainly responsible for the *de novo* DNA methylation during development [8, 9]. In mammals, *Dnmt3* subfamily is composed of three members, *Dnmt3a*, *Dnmt3b*, and *Dnmt3l* [10]. Recently, *Dnmt3c*, a novel rodent specific member of the *de novo dnmts*, has been identified to regulate DNA methylation in the male germline [11]. Of these, *Dnmt3a*, *Dnmt3b*, and *Dnmt3c* have been proven to have catalytic activities *in vivo*, whereas *Dnmt3l* is a catalytically inactive DNA methyltransferase cofactor [9, 12].

Studies on mammals have shown that *Dnmt3a*, *Dnmt3c* and *Dnmt3l*, not *Dnmt3b*, are required for gametogenesis. During the development of male germ cells in mouse, *Dnmt3a*

exhibited dynamic expression patterns and it is highly expressed in spermatogonia and spermatocytes [13, 14]. Male germ cells without *Dnmt3a* or *Dnmt3l* undergo meiotic catastrophe, impaired spermatogenesis, which results in no spermatocytes, spermatids or spermatozoa and significantly reduced testis size in *Dnmt3a* conditional mutant mouse [15-18]. In female mouse, *Dnmt3a* is expressed in follicles and stromal cells at different developmental stages, and exist in cytoplasm and nucleus of oocytes and granulosa cells [19, 20]. *Dnmt3a* or *Dnmt3l* null oocytes fail to acquire methylation during oocytes growth, which leads to abnormal embryonic development after fertilization [15, 17].

The teleost specific whole genome duplication has increased the *dnmts* copy number [21, 22]. Two *Dnmt3a* paralogous genes (*dnmt3aa* and *dnmt3ab*) have been isolated and identified in tilapia, zebrafish, flatfish and ricefield eel [21, 23-25]. Studies on *dnmt3aa* and *dnmt3ab* in fish have been mainly focused on their expression in gonads. In Nile tilapia and bluehead wrasse, the expressions of *dnmt3aa* and *dnmt3ab* are significantly higher in the testes than in the ovaries, and significantly increased during the sex reversal from female to male [21, 26]. In ricefield eel, *dnmt3aa* and *dnmt3ab* are highly expressed in spermatocytes of testes, with the expression of *dnmt3aa* significantly increased during the female to male sex reversal [25, 27]. These studies suggest that *dnmt3aa* and *dnmt3ab* may play important roles in gonadal development of fish, however, their detailed expression profiles during the sex determination and differentiation and gonadal development of teleost are unclear. Recently, some research groups reported the mutation of *dnmt3aa* and *dnmt3ab* in zebrafish, demonstrating their critical function on behavior regulation [28], temperature adaptation [29] and brain neural development [30]. Nevertheless, the roles of *dnmt3aa* and *dnmt3ab* in gonadal development of fish remain

unknown.

Nile tilapia (*Oreochromis niloticus*) is an important farmed fish with a stable XX-XY sex determination system. The availability of genetic all-XX and all-XY fish [31], short spawning cycle (14 days), together with the availability of high-quality genome sequences [32], have made it an excellent model for the study of gene expression and function in relation to reproduction and fertility. Particularly, genome editing technique has been established in tilapia by our group [33]. In the present study, we clarified the precise expression profiles of *dnmt3aa* and *dnmt3ab* during the key stages of gonadal development in female and male, uncovered their roles in reproduction and fertility in teleosts and the possible mechanism involved, by homozygous mutant establishment and phenotype analyzes in Nile tilapia.

Results

Expression patterns and cellular localization of *dnmt3aa* and *dnmt3ab* in developing gonads.

Generally, several key biological events occur at different time points during gonadal development in tilapia, such as sex determination and differentiation at 5-10 dah (day after hatching), the initiation of germ cells meiosis and oogenesis in the XX gonads (ovaries) at 30 dah, the initiation of spermatogenesis in the XY gonads (testes) at 90 dah, and sperm maturation in the XY gonads and vitellogenesis in the XX gonads at 180 dah. In this study, we analyzed the expression patterns and cellular localization of *dnmt3aa* and *dnmt3ab* in female and male gonads of tilapia from 5 to 180 dah.

Ontogeny analyses showed that *dnmt3aa* and *dnmt3ab* displayed sexually dimorphic expression profiles in developing gonads (Additional file 1: Fig. S1). *Dnmt3aa* and *dnmt3ab*

were expressed in gonads from as early as 5 dah, with relatively higher expression in the testes than the ovaries. In the testes, *dnmt3aa* was up-regulated from 5 to 180 dah. In the ovaries, *dnmt3aa* was up-regulated from 5 dah and reached the highest level at 120 dah, and maintained this level till 180 dah (Additional file 1: Fig. S1a). *Dnmt3ab* was up-regulated from 5 to 120 dah and maintained at relatively high level in ovaries and testes at 120 and 180 dah (Additional file 1: Fig. S1b). Generally, higher expression was observed for *dnmt3aa* than *dnmt3ab* at all the time point examined.

We identified the cell populations expressing *dnmt3aa* and *dnmt3ab* in gonads by fluorescence *in situ* hybridization (FISH). *dnmt3aa* was widely expressed in the gonads of tilapia, highly expressed in oogonia, phase I and II oocytes and granulosa cells of ovaries (Fig. 1a-d), spermatogonia and spermatocytes of testes (Fig. 1e-h). *Dnmt3ab* was mainly expressed in granulosa cells of ovaries (Fig. 1i-l) and spermatocytes of testes (Fig. 1m-p). In contrast, no signal for *dnmt3aa* and *dnmt3ab* mRNA was detected in the gonads using the sense probe (Additional file 1: Fig. S2).

Establishment of tilapia *dnmt3aa* and *dnmt3ab* mutant lines by CRISPR/Cas9.

The gRNA sites containing *Hpy 188*III and *Mly* I adjacent to protospacer adjacent motif (PAM) were selected in the third and second exon of *dnmt3aa* and *dnmt3ab*, respectively (Fig. 2a, b). Genomic DNA extracted from 20 pooled injected embryos was used as a template for PCR amplification and mutation assays. Complete digestion of the PCR products from *dnmt3aa* and *dnmt3ab* with *Hpy 188*III and *Mly* I, respectively, produced two fragments in the control groups, while an intact DNA fragment was observed in embryos injected with both Cas9 mRNA and target gRNA (Fig. 2a, b). Representative Sanger sequencing results from the uncleaved bands

were listed. In-frame and frame-shift deletions induced at the target sites were confirmed by Sanger sequencing (Fig. 2a, b).

F1 generation fish were obtained by crossing chimeric XY F0 males and WT XX females. Heterozygous F1 offspring with a deletion of 4 bp for *dnmt3aa* and 5 bp for *dnmt3ab*, were selected to breed the F2 generation (Fig. 2c). Further, homozygous mutant fish of *dnmt3aa* and *dnmt3ab* were validated by Sanger sequencing (Fig. 2d, e). Frame-shift mutations led to premature termination of translation of *dnmt3aa* at amino acid 126 and *dnmt3ab* at amino acid 36 (Fig. 2f, g). Restriction enzyme digestion assay identified the $dnmt3aa^{+/+}$, $dnmt3aa^{+/-}$, $dnmt3aa^{-/-}$, $dnmt3ab^{+/+}$, $dnmt3ab^{+/-}$ and $dnmt3ab^{-/-}$ individuals (Fig. 2h, i). The loss of *dnmt3aa* and *dnmt3ab* mRNA was confirmed by reverse transcription PCR (RT-PCR) using a specific primer on the target site (Fig. 2j).

Gonadal morphology and histology of $dnmt3aa^{-/-}$ and $dnmt3ab^{-/-}$ female mutants.

To investigate the role of *dnmt3aa* and *dnmt3ab* in follicular development, we analyzed the gross morphology and histology of WT, $dnmt3aa^{-/-}$ and $dnmt3ab^{-/-}$ ovaries at different developmental stages. Morphological observation showed that the $dnmt3aa^{-/-}$ ovaries atrophied at 60 dah, while there was no difference in gonad morphology between $dnmt3ab^{-/-}$ and WT (Fig. 3a-c). We selected three different sampling points (part1, part2 and part3) from $dnmt3aa^{-/-}$ ovaries, including the gonad smaller part, the thicker part and the atrophy part, for histological observation. The results showed that at 60 dah, WT and $dnmt3ab^{-/-}$ ovaries were full of oogonia, phase I and phase II oocytes, while $dnmt3aa^{-/-}$ ovaries had only a few oogonia and oocytes (Fig. 3a'-c'). Consistently, statistical analysis showed that the GSI of $dnmt3aa^{-/-}$ fish was significantly lower than that of WT fish, and the number of follicles at different developmental

146 stages was significantly reduced, while there was no significant difference between *dnmt3ab*$^{-/-}$
147 and WT fish (Fig. 3d, e).

148 To assess whether the atrophied ovaries could be recovered, we further analyzed two more
149 developmental stages at 120 dah and 240 dah. Morphological observations showed that
150 *dnmt3aa*$^{-/-}$ ovaries were atrophied and degenerated, while, *dnmt3ab*$^{-/-}$ ovaries developed
151 normally at 120 and 240 dah (Fig. 3f-h, k-m). Histological observation showed that the WT and
152 *dnmt3ab*$^{-/-}$ ovaries were filled with phase II and phase III oocytes at 120 dah, while only a few
153 phase II and phase III oocytes existed in *dnmt3aa*$^{-/-}$ ovaries (Fig. 3f'-h'). At 240 dah, the
154 oocytes of WT, *dnmt3aa*$^{-/-}$ and *dnmt3ab*$^{-/-}$ females were matured, less oogonia, phase I, phase
155 II, phase III and phase IV follicle cells was observed in *dnmt3aa*$^{-/-}$ ovaries than the *dnmt3ab*$^{-/-}$
156 and WT ovaries (Fig. 3k'-m'). Consistently, statistical analysis showed that the GSI and the
157 number of follicles of *dnmt3aa*$^{-/-}$ was significantly decreased (Fig. 3i, j, n, o). In addition, the
158 number of follicles in *dnmt3aa*$^{-/-}$ ovarian smaller part (part1) and atrophy part (part3) was also
159 significantly reduced (Additional file 1: Fig. S3). Taken together, these results suggest that
160 homozygous mutation of *dnmt3aa* resulted in reduced follicles and ovarian atrophy and
161 degeneration in tilapia.

162 **Gonadal morphology and histology of *dnmt3aa*$^{-/-}$ and *dnmt3ab*$^{-/-}$ male mutants.**

163 The gross morphology and histology of the testes in the WT, *dnmt3aa*$^{-/-}$ and *dnmt3ab*$^{-/-}$ fish
164 were analyzed at 60, 120 and 240 dah. At 60 dah, no obvious difference was observed in the
165 testicular morphology among them (Fig. 4a-c). Histological examination showed that the testes
166 of WT, *dnmt3aa*$^{-/-}$ and *dnmt3ab*$^{-/-}$ fish were full of spermatogonia (Fig. 4a'-c') and with no
167 difference in number (Fig. 4e). At 120 dah, the testes of *dnmt3aa*$^{-/-}$ fish were smaller and more

transparent than those of the WT fish (Fig. 4f-h). Histological examination showed that the testes of WT and *dnmt3ab*$^{-/-}$ fish were full of spermatogenic cells at different developmental stages, while less spermatocytes were observed in *dnmt3aa*$^{-/-}$ testes (Fig. 4f'-h'). Statistical analysis showed that the GSI and the number of spermatocytes in the testes of *dnmt3aa*$^{-/-}$ fish were significantly lower than those of WT fish (Fig. 4i, j). At 240 dah, morphological observation showed that the testes of the *dnmt3aa*$^{-/-}$ fish, but not the WT and *dnmt3ab*$^{-/-}$fish, was transparent (Fig. 4k-m). Histological examination showed that *dnmt3aa*$^{-/-}$ fish had fewer spermatocytes (Fig. 4l'), compared with the *dnmt3ab*$^{-/-}$ fish and the WT fish (Fig. 4m'). Consistently, compared with the WT fish, the GSI and spermatocytes number of *dnmt3aa*$^{-/-}$ fish were significantly reduced at 240 dah (Fig. 4n, o).

Germ cells apoptosis in *dnmt3aa*$^{-/-}$ and *dnmt3ab*$^{-/-}$ gonads.

Germ cells in the ovaries of *dnmt3aa*$^{-/-}$ fish were significantly decreased. In order to further evaluate the effect of *dnmt3aa* and *dnmt3ab* mutation on ovary development of tilapia, we examined the total and apoptotic germ cells in WT, *dnmt3aa*$^{-/-}$ and *dnmt3ab*$^{-/-}$ fish by Vasa (germ cells marker) and TUNEL immunofluorescence co-staining (Fig. 5a-o). The number of Vasa positive cells in *dnmt3aa*$^{-/-}$ ovaries was significantly reduced compared with that of WT fish, but there was no difference between *dnmt3ab*$^{-/-}$ and WT fish (Fig. 5p). TUNEL assay showed that there was a large number of germ cells in apoptosis in *dnmt3aa*$^{-/-}$ ovaries (Fig. 5j), but there was no obvious germ cells apoptosis in ovaries of the *dnmt3ab*$^{-/-}$ and WT fish (Fig. 5e, o). Statistical analysis showed that the number of apoptotic germ cells in the *dnmt3aa*$^{-/-}$ ovaries was significantly increased compared with that in the *dnmt3ab*$^{-/-}$ and WT ovaries (Fig. 5q). In zebrafish, medaka and tilapia, significant decrease of ovarian germ cells led to female

190 to male sex reversal [33-36]. Therefore, we further examined the expression of *cyp19a1a*, the
191 female pathway key gene, and found that it was still expressed in the *dnmt3aa*$^{-/-}$ ovaries
192 (Additional file 1: Fig. S4). It is worth noting that in the F0 generation mutants with high
193 mutation rate (75%) at another *dnmt3aa* target, we also observed a significant reduction of germ
194 cells in the ovaries (Additional file 1: Fig. S5).

195 Similar to the situation observed in ovaries, the number of spermatocytes in the testes of
196 *dnmt3aa*$^{-/-}$ fish decreased significantly at 120 dah. In order to further evaluate the effect of
197 *dnmt3aa* and *dnmt3ab* mutation on testes development of tilapia, we examined the total and
198 apoptotic spermatocytes in WT, *dnmt3aa*$^{-/-}$ and *dnmt3ab*$^{-/-}$ fish by Sycp3 (spermatocyte marker)
199 and TUNEL immunofluorescence co-staining (Fig. 6a-o). Statistical analysis showed that the
200 number of Sycp3 positive cells in *dnmt3aa*$^{-/-}$ fish was significantly lower than that of WT fish,
201 while no significant difference in the number of Sycp3 positive cells was observed in
202 *dnmt3ab*$^{-/-}$ and WT fish (Fig. 6p). A large number of apoptotic spermatocytes, significantly
203 higher than that of WT and *dnmt3ab*$^{-/-}$ fish, was observed in *dnmt3aa*$^{-/-}$ fish (Fig. 6j, q).

204 **Sperms quality of WT, *dnmt3aa*$^{-/-}$ and *dnmt3ab*$^{-/-}$ XY fish.**

205 The semens were obtained from the mature WT, *dnmt3aa*$^{-/-}$ and *dnmt3ab*$^{-/-}$ mutants by *in*
206 *vitro* extrusion at 240 dah, and analyzed with a computer-assisted sperm analyzer after 1:10
207 dilution. The sperms from *dnmt3aa*$^{-/-}$ mutants displayed lower activity compared with those
208 from the WT and *dnmt3ab*$^{-/-}$ fish (Fig. 7a-c). In addition, the sperm concentration of *dnmt3aa*$^{-/-}$
209 mutants was significantly lower than that of WT and *dnmt3ab*$^{-/-}$fish (Fig. 7d). Further analysis
210 showed that the percentage of progressive sperms in *dnmt3aa*$^{-/-}$ fish was significantly lower
211 than that in WT and *dnmt3ab*$^{-/-}$ fish (Fig. 7e), and the proportion of immotile sperms was

212 significantly higher than that in WT and *dnmt3ab*$^{-/-}$ fish (Fig. 7f). Furthermore, the VSL
213 (Straight linear velocity) (Fig. 7g), VCL (Curvilinear velocity) (Fig. 7h) and BCF (Beat
214 frequency of sperms flagella) (Fig. 7i) of sperms from the *dnmt3aa*$^{-/-}$ fish were significantly
215 lower than those of the WT and *dnmt3ab*$^{-/-}$ fish. Morphologically, similar to the WT sperms,
216 the sperms from the *dnmt3ab*$^{-/-}$ mutants were characterized with straight and long tail, while
217 the sperms from *dnmt3aa*$^{-/-}$ mutants consisted of some abnormal sperms with curly and short
218 tail from Papanicolaou staining and scanning electron microscope analysis (Fig. 7 j-l,
219 Additional file 1: Fig. S6).

220 **Apoptosis genes expression and compensatory expression of *dnmt* family genes in**
221 ***dnmt3aa*$^{-/-}$ and *dnmt3ab*$^{-/-}$ gonads.**

222 As mentioned above, there was a large number of germ cells in apoptosis in the gonads of
223 *dnmt3aa*$^{-/-}$ fish. Thus, we further analyzed the expression of apoptosis genes in 60 dah XX and
224 120 dah XY gonads by quantitative real time PCR (qRT-PCR). The results showed that the
225 expression of apoptosis genes *baxa*, *baxb*, *caspase3a*, *caspase3b* and *caspase8* was
226 significantly increased in *dnmt3aa*$^{-/-}$ ovaries at 60 dah, but there was no significant difference
227 between *dnmt3ab*$^{-/-}$ and WT ovaries (Fig. 8a). Gonads of *dnmt3aa* and *dnmt3ab* homozygous
228 mutants were analyzed for gene compensatory expression. The homozygous mutation of
229 *dnmt3ab* caused a compensatory increase of *dnmt3aa* expression at 60 dah. However, there was
230 no significant difference in the expression of other *dnmts* between the mutants and WT fish
231 (Fig. 8b). At 120 dah, the expression of apoptosis genes *baxa*, *baxb*, *caspase3b* and *caspase8*
232 in *dnmt3aa*$^{-/-}$ males was significantly increased (Fig. 8c). Interestingly, we found that *dnmt3aa*
233 and *dnmt3ab* compensated for each other in the homozygous mutant males at 120 dah (Fig. 8d).

The global DNA methylation level of WT, *dnmt3aa*$^{-/-}$ and *dnmt3ab*$^{-/-}$ gonads.

The global DNA methylation status in WT, *dnmt3aa*$^{-/-}$ and *dnmt3ab*$^{-/-}$ gonads was examined using 5-methylcytosine (5-mC) antibody, which could detect 5-methylcytosine but not unmethylated cytosine. Immunoreactive signals were predominantly present in the nuclei of oocytes and granulosa cells in ovaries (Fig. 9a-c) and spermatogonia, spermatocytes and spermatozoa in testes (Fig. 9d-f). The immunoreactive signals were strong in spermatocytes and spermatozoa but weak in spermatogonia (Fig. 9d-f). Statistical analysis showed that the 5-mC levels in ovaries and testes of *dnmt3aa*$^{-/-}$ fish were significantly lower than those of WT and *dnmt3ab*$^{-/-}$ fish. There were no significant differences of the 5-mC levels in ovaries and testes between *dnmt3ab*$^{-/-}$ and WT fish (Fig. 9g, h). Further analysis showed that the 5-mC levels of granulosa cells in ovaries and spermatogonia, spermatocytes and spermatozoa in testes of *dnmt3aa*$^{-/-}$ fish were significantly lower than those of *dnmt3ab*$^{-/-}$ and WT fish (Additional file 1: Fig. S7). These results showed that mutation of *dnmt3aa* significantly reduced the 5-mC levels in tilapia ovaries and testes.

Discussion

DNA methylation, mediated by *dnmts*, is required for proper embryonic development and for the formation of mature functional germ cells [38]. *Dnmt3a*, one of the *dnmts*, is responsible for *de novo* methylation of mammalian germ cells and plays crucial roles in mammalian gonads development [17, 39-40]. In teleost, there are two *Dnmt3a* paralogs, *dnmt3aa* and *dnmt3ab*, due to the third round of genome duplication [21]. The expression patterns and roles of *dnmt3aa* and *dnmt3ab* in gonadal development remain poorly understood in teleost. In the present study, we examined the expression patterns of both *dnmt3aa* and *dnmt3ab*, mutated them, and

analyzed the gonadal phenotypes and discussed possible mechanisms in the farmed fish Nile tilapia.

Different expression patterns of *dnmt3aa* and *dnmt3ab* in gonad indicate the subfunctionalization in teleost.

Gene expression patterns are important aspects of gene regulation and function analysis. The analysis of *Dnmt3a* expression patterns in gonads is mainly focused on mammals [19, 41], but rarely reported in fish. In humans, *Dnmt3a* mRNA expression is detected in the ovarian follicles from primordial to secondary follicles, granulosa cells, and germinal vesicle (GV) and metaphase II (MII) oocytes [42]. In addition, *Dnmt3a* is expressed in human spermatogenic cells, including spermatogonia cells, primary spermatocytes, secondary spermatocytes, and round spermatids [43]. In rhesus monkey, *Dnmt3a* mRNA is expressed in follicles at different developmental stages [44]. In female mouse, Dnmt3a protein is localized around the nucleus of GV oocytes and in the cytoplasm of the MII oocytes [45]. In male mouse, *Dnmt3a* is expressed at mRNA and protein levels in male germ cells, at a high level in type A spermatogonia, slightly decreased in type B spermatogonia, and further decreased in preleptotene and pachytene spermatocytes [13-14]. In general, Dnmt3a is expressed in mammalian follicles and granulosa cells of ovaries and spermatogenic cells of testes. There are few studies on the cellular localization of *dnmt3aa* and *dnmt3ab* in teleost except for a report describing immunoreactive signals for Dnmt3a (Dnmt3aa and Dnmt3ab) in male germ cells, particularly in spermatocytes in ricefield eels [25]. In this study, we comprehensively studied the expression patterns and their cellular localization of *dnmt3aa* and *dnmt3ab* in the ovaries and testes of tilapia. *Dnmt3aa* and *dnmt3ab* displayed sexually dimorphic expression profiles in developing gonads with

higher expression in testes than in ovaries. Furthermore, higher expression was observed for *dnmt3aa* than *dnmt3ab* at all the time point examined, suggesting that *dnmt3aa* may play more important roles in gonadal development than *dnmt3ab*. In tilapia, *dnmt3aa* was highly expressed in oogonia, phase I and II oocytes and granulosa cells, while *dnmt3ab* was mainly expressed in granulosa cells of the ovaries. Both were highly expressed in spermatogonia and spermatocytes of the testes. These results demonstrated that the expression of *dnmt3aa* and *dnmt3ab* in Nile tilapia was basically consistent with that in mammals. Interestingly, in ovaries, *dnmt3aa* was expressed in both germ cells (oogonia and oocytes) and somatic cells (granulosa cells), while *dnmt3ab* was only expressed in somatic cells (granulosa cells). The different expression patterns of *dnmts* in gonads are probably essential for the acquisition of a sex specific methylation pattern [46]. The different expression patterns of *dnmt3aa* and *dnmt3ab* in the gonads of tilapia suggest that they may play different roles in gonadal development of tilapia.

The function of *Dnmt3a* (*dnmt3aa* and *dnmt3ab*) in gonadal development of vertebrates

The development of germ cells in gonads is a highly ordered process, which initiate in the growth of fetus and complete in adults [6]. DNA methylation, as an important epigenetic modification, has important implications for gamete integrity and formation of functionally mature germ cells in mammals [7]. During germ cells development, DNA methylation reprogramming occurred dynamically [3, 4]. Both male and female PGCs undergo genome-wide DNA demethylation to reach a very low DNA methylation level at E13.5 [47, 48]. After E13.5, the male germ line is globally remethylated before birth, whereas the female germ line regains DNA methylation during oocytes growth after birth. During this process, *Dnmt3a* is essential for both male and female germ lines *de novo* methylation [5, 17, 49].

During follicular development after birth, DNA methylation is thought to play important roles in the regulation of gene expression in oocytes. In the process of oocytes maturation from GV to MII stages global DNA methylation gradually increases and reaches the highest level in MII oocytes [48]. Genomic imprints are established during this process [50]. Conditional knockout of *Dnmt3a* in mouse oocytes results in failure of DNA methylation establishment in oocytes, significant reduction of DNA methylation, loss of maternal imprints, and death of offspring in uterus [5, 17, 39, 49-51].

DNA methylation is also crucial for somatic granulosa cells that surround oocytes during follicular development. Granulosa cells are essential for producing competent oocytes. Correctly established DNA methylation in the granulosa cells is important for the regulation of expression of genes related to follicular development [52]. It is noteworthy that granulosa cells undergo dynamic DNA methylation changes to repress or activate the genes required for their proliferation and differentiation during follicular development in human [53, 54]. Studies in human and bovines have shown that the methylation levels of granulosa cells in ovaries decreases with age [53, 55, 56]. Abnormal DNA methylation in the granulosa cells was associated with the age-related decline of ovarian function, oocyte quality, and altered gene expression, and changing *Dnmt3a* gene expression in granulosa cells causes impaired oocyte maturation in the GV and MII oocytes and subsequent abnormal embryonic development [20, 57]. In this study, homozygous mutation of *dnmt3aa* resulted in partial gonadal degeneration, oocytes apoptosis and significant increase of apoptosis genes, suggesting that *dnmt3aa* plays important roles in the development of tilapia oocytes. In mice, oocytes conditional knockout Dnmt3a are capable to fertilize, different from the phenotype observed in tilapia in which global

mutation of *dnmt3aa* caused oocytes apoptosis and ovarian degeneration. The discrepancy might be attributed to the following reasons: (1) The oocyte does not develop in isolation but in instead highly dependent on surrounding granulosa cells of the intact ovarian follicle. The process of oocytes development is supported by granulosa cells, and the bidirectional communication between oocytes and granulosa cells is important for the development and maturation of the oocytes [58-60]. The abnormal methylation, significant decrease of 5-mC level, of granulosa cells affected the development of oocytes and resulted in oocytes apoptosis in *dnmt3aa*$^{-/-}$ mutants in tilapia. (2) Unlike viviparous mammals, fish eggs are megalecithal eggs. The oocytes development requires a large amount of yolk accumulation. Insufficient vitellogenin synthesis in liver led to oocytes development arrest and increased oocytes apoptosis in *dnmt3aa*$^{-/-}$ mutants. (3) Studies have shown that some apoptosis genes (*caspase3*, *caspase8*) are directly regulated by DNA methylation [61, 62]. Mutation of *dnmt3aa* decreased DNA methylation promoted the expression of apoptosis genes and caused the apoptosis of oocytes in tilapia.

DNA methylation also plays crucial roles in normal spermatogenesis. Previous studies have demonstrated that male germ cells in mice have a highly distinct epigenetic pattern, characterized by a unique genome-wide pattern of DNA methylation. During spermatogenesis, global remethylation is established from spermatogonia to spermatocytes, and continues in the round spermatids and spermatozoa [63, 64]. It has been reported that abnormal DNA methylation in spermatogenic cells due to genetic failure, environmental factors and disturbed expression of the *dnmts* may lead to spermatogenic impairments [65-67]. Indeed, azoospermia studies in human have shown that significant changes in *dnmts* expression and DNA

methylation levels in spermatogenic cells may lead to male infertility [68]. In male mouse, conditional mutation of *Dnmt3a* in germ cells led to meiotic catastrophe, impaired spermatogenesis and small testes with no spermatocytes, spermatids and spermatozoa [17]. In this study, significantly higher apoptotic signals (TUNEL staining) and apoptotic genes expression were observed in spermatocytes of the *dnmt3aa* mutant testes, suggesting that *dnmt3aa* plays important roles in spermatogenesis in tilapia. However, viable sperms were produced in *dnmt3aa*$^{-/-}$ fish even though the sperm concentration, motility, and flagella beat frequency were significantly lower than those of WT fish, which is different from the phenotype of Dnmt3a conditional mutation in mice. Interestingly, a significant up-regulation of *dnmt3ab* expression in *dnmt3aa*$^{-/-}$ testes was observed. The compensatory increase of *dnmt3ab* in the testes of *dnmt3aa*$^{-/-}$ mutants may be one of the reasons for these differences. In human, low sperms motility is associated with decreased sperms methylation [69]. Consistently, lower 5-mC level of spermatozoa and lower sperm mobility were observed in *dnmt3aa*$^{-/-}$ mutants of tilapia.

It is worth noting that homozygous mutation of *Dnmt3a* in mice was fatal, whereas mutation of either *dnmt3aa* or *dnmt3ab* in zebrafish and tilapia was viable [28, 29, 70]. In this study, different spatial-temporal expression profiles of *dnmt3aa* and *dnmt3ab*, up-regulation of *dnmt3ab* in *dnmt3aa*$^{-/-}$ gonad and up-regulation of *dnmt3aa* in *dnmt3ab*$^{-/-}$ gonad were observed. These results indicate the subfunctionalization and compensation of *dnmt3aa* and *dnmt3ab* in tilapia, and might be possible reasons for the survival of these mutants. As suggested previous study [71], the existence of duplicate genes probably increased the survival opportunities of the species. Our study provided another model for the notion.

Conclusions

In this study, we demonstrated that both *dnmt3aa* and *dnmt3ab* displayed sexually dimorphic expression in developing gonads. *Dnmt3aa* was highly expressed in oogonia, phase I and II oocytes and granulosa cells in ovaries and spermatogonia and spermatocytes in testes, while *dnmt3ab* was mainly expressed in ovarian granulosa cells and testicular spermatocytes. Mutation of *dnmt3aa* resulted in lower GSI, increased apoptosis of oocytes and spermatocytes and significantly reduced sperm quality, while no obvious phenotype was observed in *dnmt3ab* homozygous mutants. The level of 5-mC in *dnmt3aa*$^{-/-}$ mutants testes and ovaries decreased significantly, while there was no difference between *dnmt3ab*$^{-/-}$ mutants and WT. Our results suggest that *dnmt3aa*, not *dnmt3ab*, plays important roles in maintaining normal gametogenesis in teleost. Our results enrich the understanding of the function of DNA methylatransferase in gonads of non-mammalian vertebrates.

Methods

Animals rearing conditions

Nile tilapia (*Oreochromis niloticus*) was reared in recirculating aerated freshwater tanks at 26 °C under a natural photoperiod. All-XX progenies were obtained by crossing a pseudomale (XX male, producing sperms after hormonal sex reversal) with a normal XX female. All-XY progenies were obtained by crossing an YY super male with an XX female. Animal experiments were conducted in accordance with the regulations of Guide for Care and Use of Laboratory Animals and were approved by the Committee of Laboratory Animal Experimentation at Southwest University, China. (No. IACUC-20181015-12, 15 October 2018).

Establishment of *dnmt3aa* and *dnmt3ab* homozygous mutant line by CRISPR/Cas9

CRISPR/Cas9 was performed to knockout *dnmt3aa* and *dnmt3ab* in tilapia as described previously [33]. Briefly, the guide RNA of *dnmt3aa* and *dnmt3ab* and Cas9 mRNA were co-injected into one-cell-stage embryos at a concentration of 500 and 1000 ng/μL, respectively. Twenty injected embryos were collected 72 h after injection. Genomic DNA was extracted from pooled control and injected embryos and used to access the mutations. DNA fragments spanning the target site was amplified. The mutated sequences were analyzed by restriction enzyme digestion with *Hpy* 188III and *Mly* I and Sanger sequencing.

Heterozygous F1 offspring were obtained by F0 XY male founders mated with WT XX females. The F1 fish were genotyped by fin clip assay and the individuals with frame-shift mutations were selected. XY male and XX female siblings of F1 generation, carrying the same mutation, were mated to generate homozygous F2 mutants. The F1 mutant fish which carried

4 and 5 base-pairs deletion were used for construction of F2 *dnmt3aa* and *dnmt3ab* mutants, respectively. The *dnmt3aa* and *dnmt3ab* F2 mutants were screened using restriction enzyme digestion and Sanger sequencing. The genetic sex of each fish was determined by genotyping using sex-linked marker (marker 5) as described previously [31].

Gonad morphological and histological analysis

The fish were sampled at 60, 120 and 240 dah. Briefly, the fish were anesthetized with MS-222 (Sigma-Aldrich, St. Louis, USA) and the gonad morphology of the mutants and WT fish was imaged by stereomicroscope (Leica, Bensheim, Germany) after abdominal anatomy. Then gonads were removed and the body and gonad weight were measured on an analytical balance. The gonadosomatic index was calculated. Then the gonads were fixed in Bouin's solution for 24 h at room temperature, dehydrated and embedded in paraffin. The fixed samples were then processed as follows: serial dehydration in 70, 80 and 90% ethanol for 1.5 h each, 95% ethanol for 2 h, and 100% ethanol three times for 1 h each; sequential clearance in xylene and ethanol mixture (1:1) for 30 min and xylene twice for 30 min each; and infiltration in paraffin 2 h. The samples were sectioned at 5 μm thickness using the Leica microtome (Leica Microsystems, Wetzlar, Germany). The sections were deparaffinized, hydrated, stained with hematoxylin and eosin (H&E) as described previously [72]. Photographs were taken under Olympus BX51 light microscope (Olympus, Tokyo, Japan). Sibling WT fish were used as control for phenotype analysis.

Gene expression analyses by qRT-PCR

Gonads of the WT, *dnmt3aa*$^{-/-}$ and *dnmt3ab*$^{-/-}$ fish were dissected at different developmental

stages (5, 30, 60, 90, 120 and 180 dah) for gene expression assay. Total RNA (1.0 μg) was extracted and reverse transcribed using PrimeScript RT Master Mix Perfect Real Time Kit according to the manufacturer's instructions (Takara, Dalian, China). qRT-PCR was performed on an ABI7500 qRT-PCR machine, according to the protocol of SYBR Premix Ex TaqTM II (Takara, Dalian, China). The relative abundance of key genes in the gonad was evaluated using the formula $R = 2^{-\triangle\triangle Ct}$ [73]. The reference gene *gapdh* was used to normalize the expression values. Primer sequences used in this study were listed in Additional file 2: Table S1.

Germ cells counting

The gonads of 5 fish of each genotype (WT, *dnmt3aa*$^{-/-}$ and *dnmt3ab*$^{-/-}$ fish) were dissected at 60, 120 and 240 dah. Fixed ovaries and testes by Bouin's solution were embedded in paraffin and sectioned at 5 μm thickness. Germ cells from the median sections of testes (n=5) and different parts (part1, part2 and part3) of ovaries were counted for statistical analyses. The histological classification of the follicles and spermatogenic cells were performed as described previously [74, 75].

Immunofluorescence (IF), TUNEL assay and Immunohistochemistry (IHC)

The rabbit polyclonal antibodies (Vasa, Cyp19a1a and Sycp3) were prepared by our laboratory. The dilution and specificity of these antibodies have been analyzed previously [76-78]. For IF, Alexa Fluor 488- and 594- conjugated secondary antibodies (Invitrogen, Shanghai, China) were diluted 1:500 in blocking solution and incubated with tissue to detect the primary antibodies. The nuclei were stained by 4', 6-diamidino-2-phenylindole (DAPI) (Invitrogen, Carlsbad, USA). Apoptosis of germ cells was evaluated by staining paraffin sections of WT, *dnmt3aa*$^{-/-}$ and

443 *dnmt3ab*$^{-/-}$ mutant fish at 60 (ovaries) and 120 dah (testes) with *in situ* cell death detection kit,
444 TMR red terminal deoxynucleotidyltransferase-mediated dUTP nick-end labeling (TUNEL)
445 system (Roche, Mannheim, Germany) according to the manufacturer's protocol. Apoptotic
446 germ cells in the testes (entire median section) and ovaries (part 2) (n=5) were counted for
447 statistical analysis. Fluorescence signals were captured by confocal microscopy (Olympus
448 FV3000) (Olympus, Tokyo, Japan). The assessment of global DNA methylation in WT,
449 *dnmt3aa*$^{-/-}$ and *dnmt3ab*$^{-/-}$ gonads was performed with immunohistochemistry using the anti-
450 5-methylcytosine antibody (MABE146, Merck Millipore) according to previous reports [20,
451 25]. Photographs were taken under an Olympus BX51 light microscope (Olympus, Tokyo,
452 Japan). Finally, the positive signals were quantified using image J software (National Institutes
453 of Health, Bethesda, MD, USA) according to the instructions.

454 **Fluorescence *in situ* hybridization (FISH)**

455 The tilapia *dnmt3aa* and *dnmt3ab* open reading frames were amplified with specific primers
456 (Additional file 2: Table S1), and the amplicons were cloned into pGEM-T Easy Vector. The
457 sense and anti-sense RNA probes were labeled with digoxigenin (DIG) by *in vitro* transcription
458 using an RNA labeling kit (Roche, Mannheim, Germany). The gonads of fish were sampled at
459 indicated time. The fish gonads were fixed in 4% paraformaldehyde in PBS and processed for
460 serial paraffin sectioning at 5 μm thickness. The sections were deparaffinized, rehydrated and
461 digested with proteinase K (4 μg/mL; Roche, Mannheim, Germany) at 37 °C for 15 min,
462 followed by hybridization with DIG-labeled RNA probes at 60 °C overnight. The sections were
463 washed with 50% formamide/2×SSC for 30 min, 2×SSC for 20 min, and 0.2×SSC for 20 min.
464 The slides were incubated for 30 min at room temperature in a humidified chamber with Anti-

DIG-POD (Roche, Mannheim, Germany) diluted by 200 times in DIG2 buffer. Then the sections were washed with DIG1 buffer. After washing, the TSA Plus Fluorescein System (PerkinElmer, Boston, USA) was used for the amplification of hybridization signals. The nuclei were stained by DAPI (Invitrogen, Carlsbad, USA) staining. Fluorescence signals were captured by confocal microscopy (Olympus FV3000) (Olympus, Tokyo, Japan).

Sperm mobility analysis

Sperm concentration, sperm motility, curvilinear velocity (VCL), straight line velocity (VSL) and beat frequency of sperm flagella (BCF) were examined by computer assisted sperm analysis using the Sperm Quality Analyzer according to the manufacturer's instructions (Zoneking Software, China). Briefly, sperms collected from WT, *dnmt3aa*$^{-/-}$ and *dnmt3ab*$^{-/-}$ XY fish (n=5) at 240 dah were diluted at 1:10 with phosphate buffer saline, and one drop semen was dripped into the counting pool of the sperm counting board, and placed on the operating platform of a Leica DM500 light microscope (Leica, Bensheim, Germany).

Sperms Papanicolaou staining and scanning electron microscope analysis

Semens from WT, *dnmt3aa*$^{-/-}$ and *dnmt3ab*$^{-/-}$ fish were collected by *in vivo* extrusion and then 1 μl of drained semens mixed with 9 μl of double distilled water were applied to clean slides which were dried naturally and then stained by Papanicolaou staining. Photographs were taken under Olympus BX51 light microscope (Olympus, Tokyo, Japan). To further examine sperms morphology, semens were collected from WT, *dnmt3aa*$^{-/-}$ and *dnmt3ab*$^{-/-}$ XY fish for scanning electron microscope analysis. In brief, sperm specimens were pre-fixed using 2.5 % glutaraldehyde, rinsed three times with phosphate buffer (pH 7.2), and dehydrated in ascending graded ethanol. Then the dehydrated samples were put into a drying basket and dried with

critical point dryer. The surface of the dried samples was treated with electric conduction, and the specimens were observed under a Zeiss Evo MA/LS10 (Zeiss, Oberkochen, Germany) scanning electron microscope.

Data analyses

All data were presented as mean ± SD from at least three independent experiments. Different letters above the error bar indicate statistical differences at $P < 0.05$ as determined by one-way ANOVA followed by Tukey's post-hoc test. Statistics analyses were performed using GraphPad Prism 8 software package (GraphPad Software, La Jolla, USA). In all analyses, $P < 0.05$ was considered to be statistically significant.

Abbreviations

5-mC: 5-methylcytosine; dah: day after hatching; *dnmt*: DNA methyltransferase; FISH: Fluorescence *in situ* hybridization; GSI: gonadosomatic index; IF: immunofluorescence; IHC: Immunohistochemistry; PAM: protospacer adjacent motif; qRT-PCR: quantitative reverse transcription polymerase chain reaction; RT-PCR: reverse transcription PCR.

Ethical Approval and Consent to participate

Animal experiments were conducted in accordance with the regulations of Guide for Care and Use of Laboratory Animals and were approved by the Committee of Laboratory Animal Experimentation at Southwest University, China. (No. IACUC-20181015-12, 15 October 2018).

Consent for publication

All authors have consented to publication.

Competing interests

The authors declare that they have no competing interests.

Funding

This work was supported by grants 32072963, 31630082, 31861123001 and 31872556 from the National Natural Science Foundation of China; grants 2018YFD0900202 from the National Key Research and Development Program of China; grants CQYC201903173 and cstc2019jscx-msxmX0320 from the Chongqing Science and Technology Bureau; grant SWU114101 from Fundamental Research Funds for the Central Universities.

Authors' contributions

Wang, D.S. and Sun, L.N. conceived and designed the experiments; Wang, F.L., Qin, Z.L. and Li, Z.Q. analyzed the data; Wang, F.L., Li, Z.Q. Yang, S.Y. performed the experiments; Wang, D.S., Wang, F.L., Qin, Z.L., Li, Z.Q., Gao, T. contributed reagents/materials/analysis tools. Wang, D.S., Wang, F.L. and Sun, L.N. wrote the manuscript. All authors read and approved the manuscript.

Author details

Key Laboratory of Freshwater Fish Reproduction and Development (Ministry of Education), Key Laboratory of Aquatic Science of Chongqing, School of Life Sciences, Southwest University, 400715, Chongqing, P.R. China.

Acknowledgements

We thank Minghui, Li and Xingyong, Liu for technical assistance.

References

1. Jablonka E, Lamb MJ. The changing concept of epigenetics. Ann N Y Acad Sci. 2002; 981(1):82-96.
2. Moore LD, Le T, Fan G. DNA methylation and its basic function. Neuropsychopharmacology. 2013; 38(1):23-38.
3. Duan L, Liu Y, Wang J, Liao J, Hu J. The dynamic changes of DNA methylation in primordial germ cell differentiation. Gene. 2016; 591(2):305-12.
4. Wang X, Bhandari RK. DNA methylation reprogramming in medaka fish, a promising animal model for environmental epigenetics research. Environ Epigenet. 2020; 6(1):129-140.
5. Smallwood SA, Tomizawa S, Krueger F, Ruf N, Carli N, Segonds-Pichon A, Sato S, Hata K, Andrews SR, Kelsey G. Dynamic CpG island methylation landscape in oocytes and preimplantation embryos. Nat Genet. 2011; 43(8):811-814.
6. Kurimoto K, Saitou M. Germ cell reprogramming. Curr Top Dev Biol. 2019; 135:91-125.
7. Ortega-Recalde O, Hore TA. DNA methylation in the vertebrate germline: balancing memory and erasure. Essays Biochem. 2019; 63(6):649-61.
8. Hermann A, Goyal R, Jeltsch A. The Dnmt1 DNA-(cytosine-C5)-methyltransferase methylates DNA processively with high preference for hemimethylated target sites. J Biol Chem. 2004; 279(46):48350-9.
9. Chedin F. The *Dnmt3* family of mammalian *de novo* DNA methyltransferases. Prog Mol Biol Transl Sci. 2011; 101:255-85.
10. Jurkowska RZ, Jeltsch A. Enzymology of Mammalian DNA Methyltransferases. Adv Exp

551 Med Biol. 2016; 945:87-122.

552 11. Barau J, Teissandier A, Zamudio N, Roy S, Nalesso V, Hérault Y, Guillou F, Bourc'his D.
553 The DNA methyltransferase *Dnmt3c* protects male germ cells from transposon activity.
554 Science. 2016; 354(6314):909-912.

555 12. Bheemanaik S, Reddy YV, Rao DN. Structure, function and mechanism of exocyclic DNA
556 methyltransferases. Biochem J. 2006; 399(2):177-90.

557 13. La Salle S, Trasler JM. Dynamic expression of *Dnmt3a* and *Dnmt3b* isoforms during male
558 germ cell development in the mouse. Dev Biol. 2006; 296(1):71-82.

559 14. Xu HX, Qin JZ, Zhang KY, Zeng WX. Dynamic expression profile of DNA
560 methyltransferases in rat testis development. Pol J Vet Sci. 2015; 18(3):549-56.

561 15. Bourc'his D, Xu GL, Lin CS, Bollman B, Bestor TH. *Dnmt3l* and the establishment of
562 maternal genomic imprints. Science. 2001; 294(5551):2536-9.

563 16. Hata K, Okano M, Lei H, Li E. *Dnmt3l* cooperates with the *Dnmt3* family of *de novo* DNA
564 methyltransferases to establish maternal imprints in mice. Development. 2002;
565 129(8):1983-93.

566 17. Kaneda M, Okano M, Hata K, Sado T, Tsujimoto N, Li E, Sasaki H. Essential role for *de*
567 *novo* DNA methyltransferase *Dnmt3a* in paternal and maternal imprinting. Nature. 2004;
568 429(6994):900-3.

569 18. La Salle S, Oakes CC, Neaga OR, Bourc'his D, Bestor TH, Trasler JM. Loss of
570 spermatogonia and wide-spread DNA methylation defects in newborn male mice deficient
571 in *Dnmt3l*. BMC Dev Biol. 2007; 7:104-22.

572 19. Uysal F, Akkoyunlu G, Ozturk S. Dynamic expression of DNA methyltransferases (*Dnmts*)

573 in oocytes and early embryos. Biochimie. 2015; 116:103-13.
574 20. Uysal F, Ozturk S. The loss of global DNA methylation due to decreased *Dnmt* expression
575 in the postnatal mouse ovaries may associate with infertility emerging during ovarian aging.
576 Histochem Cell Biol. 2020; 154(3), 301-314.
577 21. Wang FL, Yan LX, Shi HJ, Liu XY, Zheng QY, Sun LN, Wang DS. Genome-wide
578 identification, evolution of DNA methyltransferases and their expression during gonadal
579 development in Nile tilapia. Comp Biochem Phys B. 2018; 226:73-84.
580 22. Liu J, Hu H, Panserat S, Marandel L. Evolutionary history of DNA methylation related
581 genes in chordates: new insights from multiple whole genome duplications. Sci Rep. 2020;
582 10(1):970-84.
583 23. Campos C, Valente LMP, Fernandes JMO. Molecular evolution of zebrafish *dnmt3* genes
584 and thermal plasticity of their expression during embryonic development. Gene. 2012;
585 500(1):93-100.
586 24. Firmino J, Carballo C, Armesto P, Campinho MA, Power DM, Manchado M. Phylogeny,
587 expression patterns and regulation of DNA Methyltransferases in early development of the
588 flatfish, *Solea senegalensis*. BMC Dev Biol. 2017; 17(1):11-25.
589 25. Zhang Y, Sun X, Zhang L, Zhang W. Testicular *Dnmt3* expression and global DNA
590 methylation are down-regulated by gonadotropin releasing hormones in the ricefield eel
591 *Monopterus albus*. Sci Rep. 2017; 7:43158.
592 26. Todd EV, Ortega-Recalde O, Liu H, Lamm MS, Rutherford KM, Cross H, Black MA,
593 Kardailsky O, Marshall Graves JA, Hore TA, et al. Stress, novel sex genes, and epigenetic
594 reprogramming orchestrate socially controlled sex change. Sci Adv. 2019; 5(7):eaaw7006.

595 27. Wang X, Lai FL, Xiong J, Zhu W, Yuan BF, Cheng HH, Zhou RJ. DNA methylation
596 modification is associated with gonadal differentiation in *Monopterus albus*. Cell Biosci.
597 2020; 10(1):129-40.
598 28. Lai YH, Audira G, Liang ST, Siregar P, Suryanto ME, Lin HC, Villalobos O, Villaflores
599 OB, Hao EW, Lim KH, et al. Duplicated *dnmt3aa* and *dnmt3ab* DNA Methyltransferase
600 Genes Play Essential and Non-Overlapped Functions on Modulating Behavioral Control in
601 Zebrafish. Genes. 2020; 11(11):1322-1354.
602 29. Loughland I, Little A, Seebacher F. DNA methyltransferase 3a mediates developmental
603 thermal plasticity. BMC Biol. 2021; 19(1):11-22.
604 30. Ross SE, Hesselson D, Bogdanovic O. Developmental Accumulation of Gene Body and
605 Transposon Non-CpG Methylation in the Zebrafish Brain. Front Cell Dev Biol. 2021;
606 9:643603-643614.
607 31. Sun YL, Jiang DN, Zeng S, Hu CJ, Ye K, Yang C, Yang SJ, Li MH, Wang DS. Screening
608 and characterization of sex-linked DNA markers and marker-assisted selection in the Nile
609 tilapia (*Oreochromis niloticus*). Aquaculture. 2014; 433:19-27.
610 32. Brawand D, Wagner CE, Li YI, Malinsky M, Keller I, Fan S, Simakov O, Ng AY, Lim ZW,
611 Bezault E, et al. The genomic substrate for adaptive radiation in African cichlid fish. Nature.
612 2014; 513(7518):375-81.
613 33. Li M, Yang H, Zhao J, Fang L, Shi H, Li M, Sun Y, Zhang X, Jiang D, Zhou L, et al.
614 Efficient and heritable gene targeting in tilapia by CRISPR/Cas9. Genetics. 2014;
615 197(2):591-599.
616 34. Kossack ME, Draper BW. Genetic regulation of sex determination and maintenance in

617 zebrafish (*Danio rerio*). Curr Top Dev Biol. 2019; 134:119-49.
618 35. Schartl M. A comparative view on sex determination in medaka. Mech Dev. 2004; 121(7-
619 8):639-45.
620 36. Nishimura T, Tanaka M. The Mechanism of Germline Sex Determination in Vertebrates.
621 Biol Reprod. 2016; 95(1):30-46.
622 37. Smith ZD, Meissner A. DNA methylation: roles in mammalian development. Nat Rev
623 Genet. 2013; 14(3):204-220.
624 38. Chen Z, Zhang Y. Role of Mammalian DNA Methyltransferases in Development. Annu
625 Rev Biochem. 2020; 89:135-58.
626 39. Kaneda M, Hirasawa R, Chiba H, Okano M, Li E, Sasaki H. Genetic evidence for *Dnmt3a*-
627 dependent imprinting during oocyte growth obtained by conditional knockout with *Zp3-*
628 *Cre* and complete exclusion of *Dnmt3b* by chimera formation. Genes Cells. 2010;
629 15(3):169-79.
630 40. Yaman R, Grandjean V. Timing of entry of meiosis depends on a mark generated by DNA
631 methyltransferase 3a in testis. Mol Reprod Dev. 2010; 73(3):390-397.
632 41. Uysal F, Akkoyunlu G, Ozturk S. DNA methyltransferases exhibit dynamic expression
633 during spermatogenesis. Reprod Biomed Online. 2016;33(6):690-702.
634 42. Huntriss J, Hinkins M, Oliver B, Harris SE, Beazley JC, Rutherford AJ, Gosden RG,
635 Lanzendorf SE, Picton HM. Expression of mRNAs for DNA methyltransferases and
636 methyl-CpG-binding proteins in the human female germ line, preimplantation embryos,
637 and embryonic stem cells. Mol Reprod Dev. 2004; 67(3):323-36.
638 43. Marques CJ, João Pinho M, Carvalho F, Bièche I, Barros A, Sousa M. DNA methylation

639 imprinting marks and DNA methyltransferase expression in human spermatogenic cell
640 stages. Epigenetics. 2011; 6(11):1354-61.
641 44. Vassena R, Dee Schramm R, Latham KE. Species-dependent expression patterns of DNA
642 methyltransferase genes in mammalian oocytes and preimplantation embryos. Mol Reprod
643 Dev. 2005; 72(4):430-436.
644 45. Uysal F, Ozturk S, Akkoyunlu G. *Dnmt1*, *Dnmt3a* and *Dnmt3b* proteins are differently
645 expressed in mouse oocytes and early embryos. J Mol Histol. 2017; 48(5-6): 417-426.
646 46. La Salle S, Mertineit C, Taketo T, Moens PB, Bestor TH, Trasler JM. Windows for sex-
647 specific methylation marked by DNA methyltransferase expression profiles in mouse germ
648 cells. Dev Biol. 2004; 268(2), 403-15.
649 47. Guibert S, Forné T, Weber M. Global profiling of DNA methylation erasure in mouse
650 primordial germ cells. Genome Res. 2012; 22(4); 633-41.
651 48. Smallwood SA, Kelsey G. *De novo* DNA methylation: a germ cell perspective. Trends
652 Genet. 2012; 28(1):33-42.
653 49. Shirane K, Toh H, Kobayashi H, Miura F, Chiba H, Ito T, Kono T, Sasaki H. Mouse oocyte
654 methylomes at base resolution reveal genome-wide accumulation of non-CpG methylation
655 and role of DNA methyltransferases. Plos Genet. 2013; 9(4):e1003439.
656 50. Tomizawa S, Nowacka-Woszuk J, Kelsey G. DNA methylation establishment during
657 oocyte growth: mechanisms and significance. Int J Dev Biol. 2012; 56(10-12):867-75.
658 51. Li Y, Zhang Z, Chen J, Liu W, Lai W, Liu B, Li X, Liu L, Xu S, Dong Q, et al. Stella
659 safeguards the oocyte methylome by preventing *de novo* methylation mediated by DNMT1.
660 Nature. 2018; 564(7734):136-40.

661 52. Uysal F, Ozturk S. DNA Methyltransferases in Mammalian Oocytes. Results Probl Cell
662 Differ. 2017; 63:211-22.
663 53. Yu B, Russanova VR, Gravina S, Hartley S, Mullikin JC, Ignezweski A, Graham J, Segars
664 JH, DeCherney AH, Howard BH. DNA methylome and transcriptome sequencing in human
665 ovarian granulosa cells links age-related changes in gene expression to gene body
666 methylation and 3'-end GC density. Oncotarget. 2015; 6(6):3627-43.
667 54. Sagvekar P, Kumar P, Mangoli V, Desai S, Mukherjee S. DNA methylome profiling of
668 granulosa cells reveals altered methylation in genes regulating vital ovarian functions in
669 polycystic ovary syndrome. Clin Epigenetics. 2019; 11(11):61-77.
670 55. Goto H, Iwata H, Takeo S, Nisinosono K, Murakami S, Monji Y, Kuwayama T. Effect of
671 bovine age on the proliferative activity, global DNA methylation, relative telomere length
672 and telomerase activity of granulosa cells. Zygote. 2013; 21(3):256-64.
673 56. Olsen KW, Castillo-Fernandez J, Zedeler A, Freiesleben NC, Bungum M, Chan AC,
674 Cardona A, Perry JRB, Skouby SO, Borup R, et al. A distinctive epigenetic ageing profile
675 in human granulosa cells. Hum Reprod. 2020; 35(6):1332-45.
676 57. Fang Y, Zhang X, Zhang J, Zhong R, Zhou D. Global DNA methylation and related mRNA
677 profiles in sheep oocytes and early embryos derived from pre-pubertal and adult donors.
678 Anim Reprod Sci. 2016; 164:144-51.
679 58. Eppig JJ, Chesnel F, Hirao Y, O'Brien MJ, Pendola FL, Watanabe S, Wigglesworth K.
680 Oocyte control of granulosa cell development: how and why. Hum Reprod. 1997;
681 12(11):127-32.
682 59. Albertini DF, Barrett SL. Oocyte-somatic cell communication. Reprod Suppl. 2003; 61:49-

683 54.

684 60. Cecconi S, Ciccarelli C, Barberi M, Macchiarelli G, Canipari R. Granulosa cell-oocyte
685 interactions. Eur J Obstet Gynecol Reprod Biol. 2004; 115 Suppl 1:S19-22.

686 61. Hervouet E, Vallette FM, Cartron PF. Impact of the DNA methyltransferases expression on
687 the methylation status of apoptosis-associated genes in glioblastoma multiforme. Cell
688 Death Dis. 2010; 1(1):e8.

689 62. Gopisetty G, Ramachandran K, Singal R. DNA methylation and apoptosis. Mol Immunol.
690 2006; 43(11):1729-40.

691 63. Boissonnas CC, Jouannet P, Jammes H. Epigenetic disorders and male subfertility. Fertil
692 Steril. 2013; 99(3):624-31.

693 64. Cui X, Jing X, Wu X, Yan M, Li Q, Shen Y, Wang Z. DNA methylation in spermatogenesis
694 and male infertility. Exp Ther Med. 2016; 12(4):1973-1979.

695 65. Rajender S, Avery K, Agarwal A. Epigenetics, spermatogenesis and male infertility. Mutat
696 Res. 2011; 727(3):62-71.

697 66. Santi D, De Vincentis S, Magnani E, Spaggiari G. Impairment of sperm DNA methylation
698 in male infertility: a meta-analytic study. Andrology. 2017; 5(4):695-703.

699 67. Cheung S, Parrella A, Rosenwaks Z, Palermo GD. Genetic and epigenetic profiling of the
700 infertile male. PLoS One. 2019; 14(3):e0214275.

701 68. Uysal F, Akkoyunlu G, Ozturk S. Decreased expression of DNA methyltransferases in the
702 testes of patients with non-obstructive azoospermia leads to changes in global DNA
703 methylation levels. Reprod Fertil Dev. 2019. 31, 1386-1394.

704 69. Pacheco SE, Houseman EA, Christensen BC, Marsit CJ, Kelsey KT, Sigman M,

705 Boekelheide K. Integrative DNA methylation and gene expression analyses identify DNA
706 packaging and epigenetic regulatory genes associated with low motility sperm. PLoS One.
707 2011; 6(6):e20280.
708 70. Okano M, Bell DW, Haber DA, Li E. DNA methyltransferases Dnmt3a and Dnmt3b are
709 essential for *de novo* methylation and mammalian development. Cell. 1999; 99(3):247-257.
710 71. Lynch M, Force A. The probability of duplicate gene preservation by subfunctionalization.
711 Genetics. 2000; 154(1):459-73.
712 72. Wang DS, Kobayashi T, Zhou LY, Paul-Prasanth B, Ijiri S, Sakai F, Okubo K, Morohashi
713 K, Nagahama Y. *Foxl2* up-regulates aromatase gene transcription in a female-specific
714 manner by binding to the promoter as well as interacting with ad4 binding
715 protein/steroidogenic factor 1. Mol Endocrinol. 2007; 21(3):712-25.
716 73. Livak KJ, Schmittgen TD. Analysis of relative gene expression data using real-time
717 quantitative PCR and the 2(-Delta Delta C(T)) Method. Methods. 2001; 25(4):402-408.
718 74. Coward K, Bromage NR. Histological classification of oocyte growth and the dynamics of
719 ovarian recrudescence in Tilapia zillii. J Fish Biol. 1998; 53:285-302.
720 75. Vilela D, Silva S, Peixoto M, Godinho HP, FranA LR. Spermatogenesis in teleost: insights
721 from the Nile tilapia (*Oreochromis niloticus*) model. Fish Physiol Biochem. 2003; 28:187-
722 90.
723 76. Liu G, Luo F, Song Q, Wu L, Qiu Y, Shi H, Wang D, Zhou L. Blocking of progestin action
724 disrupts spermatogenesis in Nile tilapia (*Oreochromis niloticus*). J Mol Endocrinol. 2014;
725 53(1):57-70.
726 77. Zhang X, Li M, Ma H, Liu X, Shi H, Li M, Wang D. Mutation of *foxl2* or *cyp19a1a* results

727 in female to male sex reversal in XX Nile tilapia. Endocrinology. 2017; 158(8):2634-47.
728 78. Li M, Liu X, Dai S, Xiao H, Qi S, Li Y, Zheng Q, Jie M, Cheng CHK, Wang D. Regulation
729 of spermatogenesis and reproductive capacity by *Igf3* in tilapia. Cell Mol Life Sci. 2020;
730 77(23):4921-38.
731

Figure Legends

Fig. 1 Cellular localization of *dnmt3aa* (**a-h**) and *dnmt3ab* (**i-p**) in developing gonads by fluorescence *in situ* hybridization. *Dnmt3aa* was widely expressed in the gonads of tilapia, especially in oogonia, phase I and II oocytes and granulosa cells of ovaries (**a-d**), spermatogonia and spermatocytes of testes (**e-h**). *Dnmt3ab* was mainly expressed in granulosa cells of ovaries (**i-l**), and spermatocytes of testes (**m-p**). OC, oocytes; OG, oogonia; GC, granulosa cells; SC, spermatocytes; SG, spermatogonia; dah, day after hatching. Red fluorescence represents the *dnmt3aa* and *dnmt3ab* signals. Blue fluorescence represents the DAPI signals. Arrow indicate the positive signals. White boxes indicate the regions magnified in d and i.

Fig. 2 Establishment of *dnmt3aa* and *dnmt3ab* mutant lines. (**a**, **b**) Gene structure of *dnmt3aa* and *dnmt3ab* showing the target site and the *Hpy* 188III and *Mly* I restriction site. The Cas9 mRNA and gRNA were added as indicated. Sanger sequencing results from the uncleaved bands were listed. The PAM was marked in light green. Deletions were marked by dashes (-) and numbers to the right of the sequences in parentheses indicated the loss of bases for each allele. The mutant fish which carried 4 and 5 base-pairs deletion were used for homozygous mutant construction of *dnmt3aa* and *dnmt3ab*, respectively. WT, wild type. (**c**) Schematic diagram showing the breeding plans of *dnmt3aa* and *dnmt3ab* F0 to F2 fish. (**d**, **e**) Sequencing results of *dnmt3aa* and *dnmt3ab* genes from WT and homozygous mutant fish. (**f**, **g**) Schematic diagram of Dnmt3aa and Dnmt3ab wild type (WT) and the predicted truncated protein. (**h**, **i**) Identification of F2 genotypes by restriction enzyme digestion assay. (**j**) RT-PCR analysis of *dnmt3aa* and *dnmt3ab* mRNA expression in gonads of mutants and WT fish. The 3' sequences of forward primer were designed on the target site, which is indicated by white box. No band

was amplified in the homozygous mutants, while one band corresponding to *dnmt3aa* and *dnmt3ab* mRNA was amplified in the WT XY testes. *gapdh* was used as internal control.

Fig. 3 Morphological and histological analyses of WT, *dnmt3aa*$^{-/-}$ and *dnmt3ab*$^{-/-}$ ovaries at 60, 120 and 240 dah. (**a-c**, **a**'-**c**', **f-h**, **f**'-**h**', **k-m**, **k**'-**m**') Morphological and histological observation. (**d**, **i**, **n**) Gonadosomatic index (GSI) (n=10). (**e**, **j**, **o**) Statistical analysis of germ cells counting (n=5). Follicles from the median sections (part2) of ovaries were counted for statistical analyses. (**a-c**, **f-h**） Gonads were fixed with Bouin's solution. Different letters above the error bar indicate statistical differences at $P < 0.05$ as determined by one-way ANOVA followed by Tukey's post-hoc test. Results were presented as mean ± SD in d, e, i, j, n and o. Scale bar in a-c, f-h, k-m, 1 cm. dah, day after hatching; OC, oocytes; OG, oogonia; GC, granulosa cells.

Fig. 4 Morphological and histological analyses of WT, *dnmt3aa*$^{-/-}$ and *dnmt3ab*$^{-/-}$ testes at 60, 120 and 240 dah. (**a-c**, **a'-c'**, **f-h**, **f'-h'**, **k-m**, **k'-m'**) Morphological and histological observation. (**d**, **i**, **n)** Gonadosomatic index (GSI) (n=10). (**e**, **j**, **o)** Statistical analysis of germ cells counting (n = 5). Germ cells from the median sections of testes were counted for statistical analyses. (**a-c**) Gonads were fixed with Bouin's solution. Different letters above the error bar indicates statistical differences at $P < 0.05$ as determined by one-way ANOVA followed by Tukey's post-hoc test. Results were presented as mean ± SD in d, e, i, j, n and o. Scale bar in a-c, f-h, k-m, 1 cm. Scale bar in a'-c', f'-h', k'-m', 10 μm. dah, day after hatching; PSC, primary spermatocytes; SG, spermatogonia; SPT, spermatids; SPZ, spermatozoa; SSC, secondary spermatocytes.

Fig. 5 Apoptosis detection in WT, *dnmt3aa*$^{-/-}$ and *dnmt3ab*$^{-/-}$ ovaries at 60 dah. Increased

apoptosis of germ cells in the ovaries of *dnmt3aa*$^{-/-}$ fish at 60 dah. (**a**, **f**, **k**) Histological analyses of germ cell by H&E staining. (**b**, **g**, **l**) Nuclei were counterstained with DAPI. (**c**, **h**, **m**) Green fluorescence represents the Vasa signals. (**d**, **i**, **n**) Red fluorescence represents the TUNEL positive signals. (**e**, **j**, **o**) Co-localization of some Vasa and TUNEL signals as indicated by orange color in tilapia ovaries. (**p**) Germ cells count of WT, *dnmt3aa*$^{-/-}$ and *dnmt3ab*$^{-/-}$ ovaries at 60 dah. (**q**) TUNEL positive germ cells in the median section of the ovaries (part2) (n=5). Results were presented as mean ± SD. Different letters above the error bar indicate statistical differences at $P < 0.05$ as determined by one-way ANOVA followed by Tukey's post-hoc test. dah, day after hatching. Scale bar, 10 μm.

Fig. 6 Apoptosis detection in WT, *dnmt3aa*$^{-/-}$ and *dnmt3ab*$^{-/-}$ testes at 120 dah. Increased apoptosis of spermatocytes in the testes of *dnmt3aa*$^{-/-}$ fish at 120 dah. (**a**, **f**, **k**) Histological analyses of germ cell by H&E staining. (**b**, **g**, **l**) Nuclei were counterstained with DAPI. (**c**, **h**, **m**) Green fluorescence represents the Sycp3 signals. (**d**, **i**, **n**) Red fluorescence represents the TUNEL positive signals. (**e**, **j**, **o**) Co-localization of some Sycp3 and TUNEL signals as indicated by orange color in tilapia testes. (**p**) Sycp3 positive cells count of WT, *dnmt3aa*$^{-/-}$ and *dnmt3ab*$^{-/-}$ testes at 120 dah. (**q**) TUNEL positive cells in the entire median section of the testes (n=5). Results were presented as mean ± SD. Different letters above the error bar indicate statistical differences at $P < 0.05$ as determined by one-way ANOVA followed by Tukey's post-hoc test. dah, day after hatching. Scale bar, 10 μm.

Fig. 7 Sperms quality analyses of WT, *dnmt3aa*$^{-/-}$ and *dnmt3ab*$^{-/-}$ XY fish at 240 dah. (**a-c**) The tracks of motile sperms from WT, *dnmt3aa*$^{-/-}$ and *dnmt3ab*$^{-/-}$ XY fish. Pink, blue and green present grade A, B, C sperms, respectively. (**d-i**) The physiological characteristics of WT,

797 *dnmt3aa*$^{-/-}$ and *dnmt3ab*$^{-/-}$ sperms (n=5). PR, progressive sperms; IM, immotile sperms. VSL,
798 straight linear velocity; VCL, curvilinear velocity; BCF, Beat frequency of sperms flagella.
799 Results were presented as mean ± SD. Different letters above the error bar indicate statistical
800 differences at $P < 0.05$ as determined by one-way ANOVA followed by Tukey's post-hoc test.
801 (**j-l**) Sperms morphology examination by scanning electron microscope.

802 **Fig. 8** Detection of apoptosis genes and analysis of compensatory expression of *dnmt* family
803 genes in *dnmt3aa*$^{-/-}$ and *dnmt3ab*$^{-/-}$ fish at 60 dah (**a**, **b**) and 120 dah (**c**, **d**). WT, wild type. The
804 reference gene *gapdh* was used to normalize the expression values. Results were presented as
805 mean ± SD. Different letters above the error bar indicate statistical differences at $P < 0.05$ as
806 determined by one-way ANOVA followed by Tukey's post-hoc test. dah, day after hatching.

807 **Fig. 9** 5-methylcytosine (5-mC) staining of WT, *dnmt3aa*$^{-/-}$ and *dnmt3ab*$^{-/-}$ gonads at 120 dah**.**
808 (**a-c**) 5-mC staining of WT, *dnmt3aa*$^{-/-}$ and *dnmt3ab*$^{-/-}$ ovaries. Positive signals were observed
809 in the nuclei of oocytes and granulosa cells. (**d-f**) 5-mC staining of WT, *dnmt3aa*$^{-/-}$ and
810 *dnmt3ab*$^{-/-}$ testes. Positive signals were observed in spermatogonia, spermatocytes and
811 spermatozoa. The positive signals correspond to the brownish color. (**g**) Statistical analysis of
812 relative 5-mC staining level in WT, *dnmt3aa*$^{-/-}$ and *dnmt3ab*$^{-/-}$ovaries. (**h**) Statistical analysis
813 of relative 5-mC staining level in WT, *dnmt3aa*$^{-/-}$ and *dnmt3ab*$^{-/-}$testes (n = 5, and five sections
814 were counted per sample). The IHC positive signals were quantified using image J software
815 according to the instructions. Results were presented as mean ± SD. Different letters above the
816 error bar indicate statistical differences at $P < 0.05$ as determined by one-way ANOVA followed
817 by Tukey's post-hoc test. OC, oocytes; GC, granulosa cells; SC, spermatocytes; SG,
818 spermatogonia; SZ, spermatozoa. Scale bar, 10 μm.

819

Fig. 1

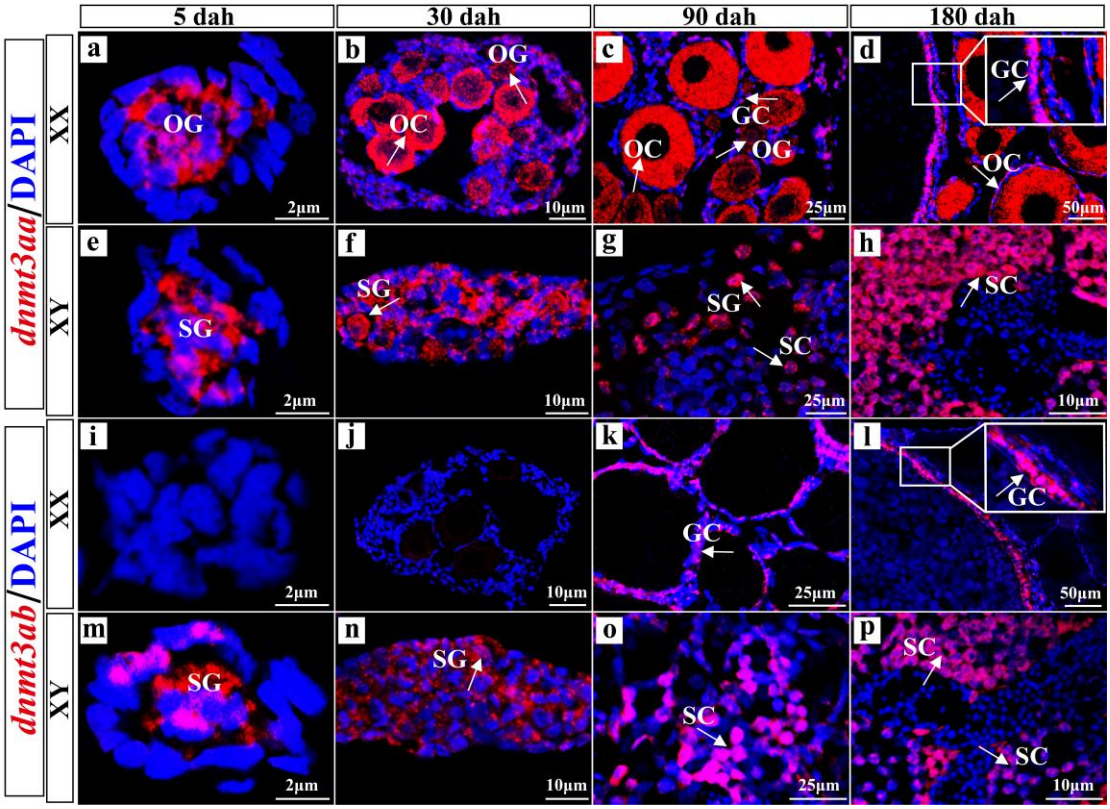
5 dah
30 dah
90 dah
180 dah
dnmt3aa/DAPI
dnmt3ab/DAPI
XX
XY
a
b
c
d
e
f
g
h
i
j
k
l
m
n
o
p
OG
OC
GC
SG
SC
2μm
10μm
25μm
50μm

Fig. 2

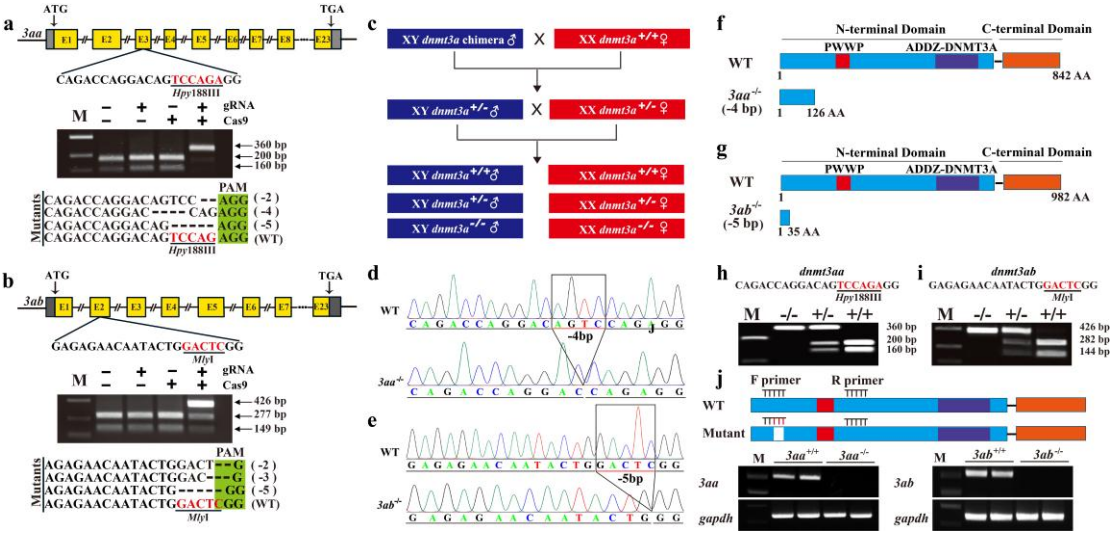
a
ATG
TGA
3aa
E1
E2
E3
E4
E5
E6
E7
E8
E23
CAGACCAGGACAGTCCAGG
Hpy188III
M
gRNA
Cas9
360 bp
200 bp
160 bp
PAM
Mutants
CAGACCAGGACAGTCC--AGG (-2)
CAGACCAGGAC----CAGAGG (-4)
CAGACCAGGACAG------AGG (-5)
CAGACCAGGACAGTCCAG AGG (WT)
b
3ab
GAGAGAACAATACTGGACTCGG
MlyI
426 bp
277 bp
149 bp
AGAGAACAATACTGGACT--G (-2)
AGAGAACAATACTGGAC---G (-3)
AGAGAACAATACTG-----GG (-5)
AGAGAACAATACTGGACTCGG (WT)
c
XY dnmt3a chimera ♂
XX dnmt3a+/+♀
XY dnmt3a+/- ♂
XX dnmt3a+/- ♀
XY dnmt3a+/+♂
XX dnmt3a+/+♀
XY dnmt3a+/- ♂
XX dnmt3a+/- ♀
XY dnmt3a-/- ♂
XX dnmt3a-/- ♀
d
WT
-4bp
3aa-/-
e
WT
-5bp
3ab-/-
f
N-terminal Domain
C-terminal Domain
PWWP
ADDZ-DNMT3A
WT
842 AA
3aa-/- (-4 bp)
126 AA
g
N-terminal Domain
C-terminal Domain
PWWP
ADDZ-DNMT3A
WT
982 AA
3ab-/- (-5 bp)
35 AA
h
dnmt3aa
CAGACCAGGACAGTCCAGAGG
Hpy188III
M -/- +/- +/+
360 bp
200 bp
160 bp
i
dnmt3ab
GAGAGAACAATACTGGACTCGG
MlyI
M -/- +/- +/+
426 bp
282 bp
144 bp
j
F primer
R primer
WT
Mutant
M 3aa+/+ 3aa-/-
3aa
gapdh
M 3ab+/+ 3ab-/-
3ab
gapdh

825 **Fig. 3**

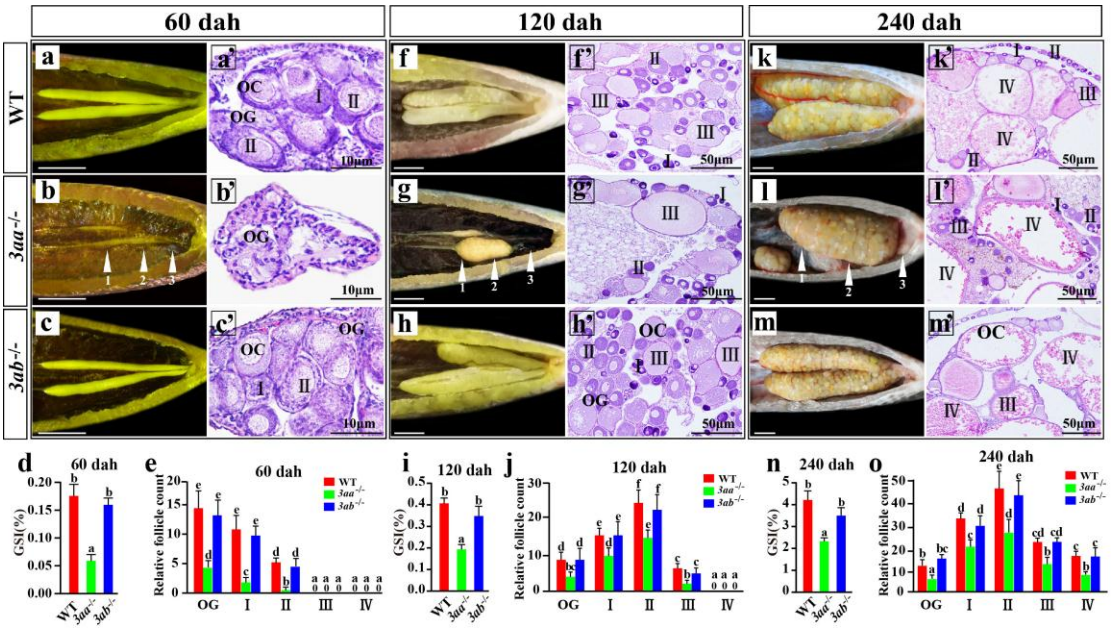
60 dah
120 dah
240 dah
WT
3aa-/-
3ab-/-
OC
OG
I
II
III
IV
10μm
50μm
GSI(%)
Relative follicle count
WT
3aa-/-
3ab-/-

826

827 **Fig. 4**

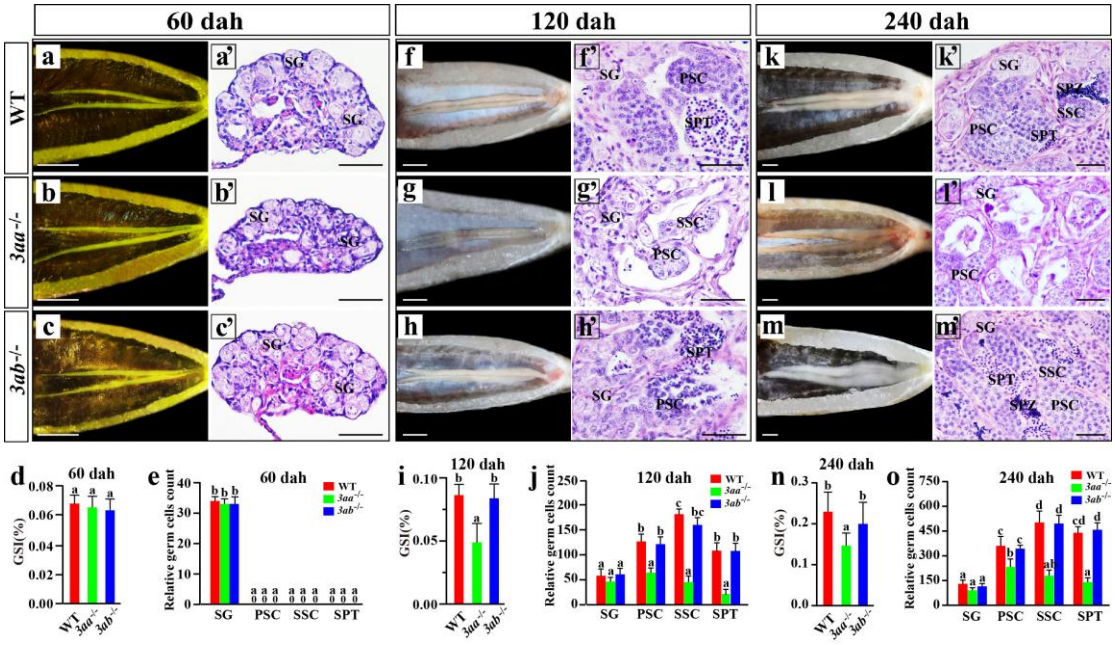

828

829

Fig. 5

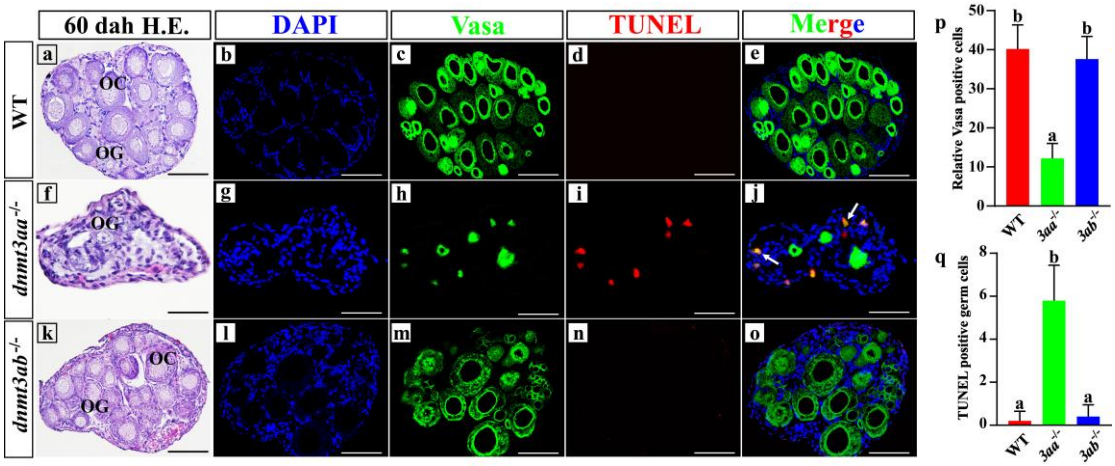
60 dah H.E.
DAPI
Vasa
TUNEL
Merge
WT
dnmt3aa-/-
dnmt3ab-/-
OC
OG
p
Relative Vasa positive cells
q
TUNEL positive germ cells
WT
3aa-/-
3ab-/-

833 **Fig. 6**

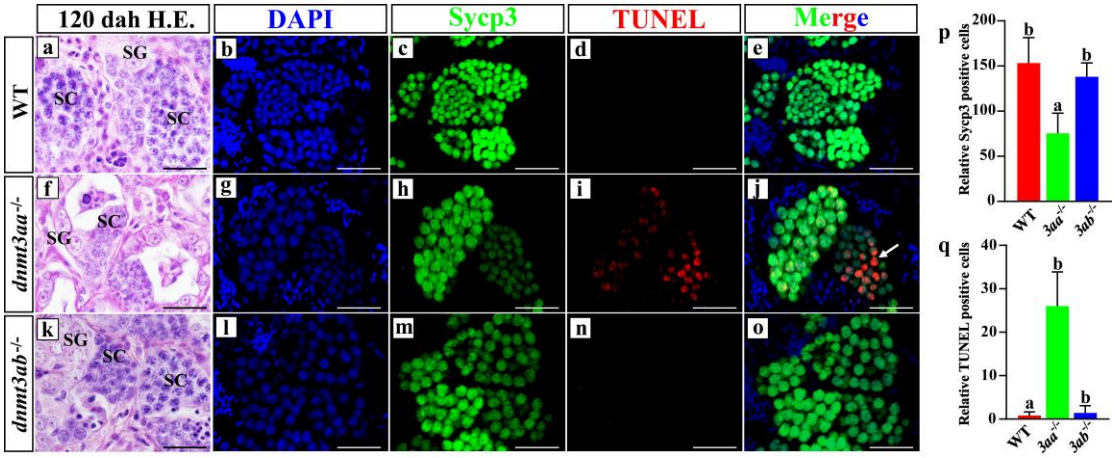

834

835

Fig. 7

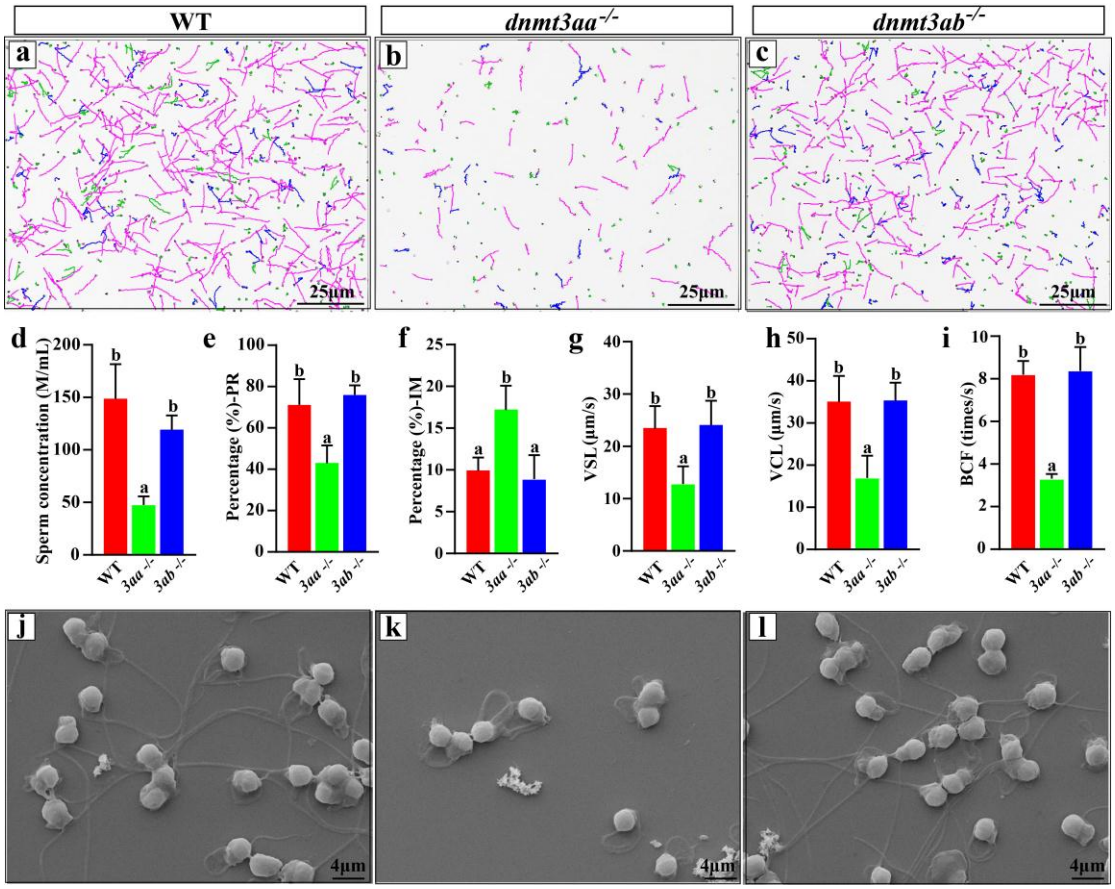
WT
dnmt3aa-/-
dnmt3ab-/-
a
b
c
25μm
d
Sperm concentration (M/mL)
e
Percentage (%)-PR
f
Percentage (%)-IM
g
VSL (μm/s)
h
VCL (μm/s)
i
BCF (times/s)
WT
3aa-/-
3ab-/-
j
k
l
4μm

839 **Fig. 8**

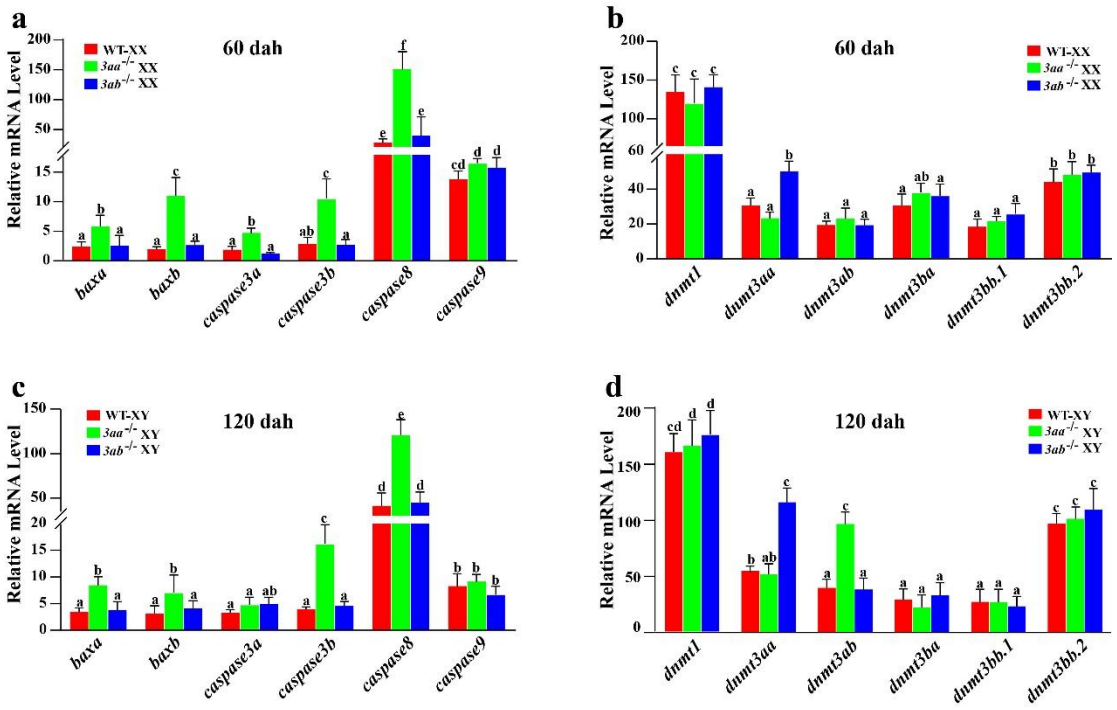

840

841 **Fig. 9**

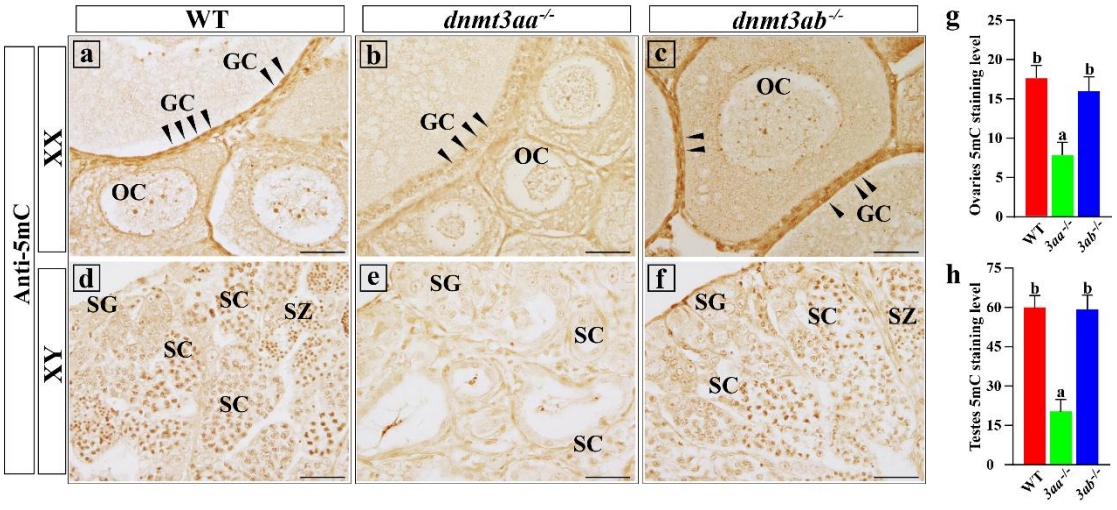

842

843

Additional file 1: Figure legends

Fig. S1 (**a-b**) Ontogenetic expression of *dnmt3aa* and *dnmt3ab* by qRT-PCR. Results were presented as mean ± SD. *gapdh* was selected as the internal control. Different letters above the error bar indicate statistical differences at $P < 0.05$, as determined by one-way ANOVA followed by Tukey's post-hoc test. dah, day after hatching.

Fig. S2 (**a-p**) Cellular localization of *dnmt3aa* and *dnmt3ab* in tilapia testes and ovaries at different developmental stages by FISH. No signal for *dnmt3aa* and *dnmt3ab* were detectable in the ovaries and testes using the sense probe. dah, day after hatching.

Fig. S3 (**a-d**, **f-i**, **k-n**) Histological observation WT and *dnmt3aa*$^{-/-}$ ovaries of part1 and part3 at 60, 120 and 240 dah. (**e**, **j**, **o**) Statistical analysis the number of WT and *dnmt3aa*$^{-/-}$ part1 and part3 ovarian follicles at 60, 120 and 240 dah. Results were presented as mean ± SD. Different letters above the error bar indicate statistical differences at $P < 0.05$ as determined by one-way ANOVA followed by Tukey's post-hoc test. dah, day after hatching.

Fig. S4 Expression analysis of *cyp19a1a* (female pathway key gene) in WT (**a-c**) and *dnmt3aa*$^{-/-}$ ovaries (**d-f**). Green fluorescence represents the Cyp19a1a signals (white arrows). Blue fluorescence represents the DAPI signals.

Fig. S5 Knockdown *dnmt3aa* by CRISPR/Cas9 in another target site. (**a**) Gene structures of *dnmt3aa* showing the second target site and the *Sau 96*I restriction site. The Cas9 mRNA and gRNA were added as indicated. Sanger sequencing results from the uncleaved bands were listed. The PAM was marked in light green. (**b-d**) Histological analysis ovaries of WT and *dnmt3aa* highly efficient knockdown females. (**e-g**) Analysis of Vasa (germ cells marker) expression in WT and *dnmt3aa* knockdown ovaries by IF. Green fluorescence represents the Vasa signals.

Blue fluorescence represents the DAPI signals. (**h**) Statistical analysis the germ cells number of WT and *dnmt3aa* knockdown fish (n=5). Results were presented as mean ± SD. ** p< 0.01.

Fig. S6 Papanicolaou staining analysis of WT, *dnmt3aa*$^{-/-}$ and *dnmt3ab*$^{-/-}$ sperms. d, e, f are the amplification of a, b and c, respectively.

Fig. S7 (**a**) Statistical analysis relative 5-mC staining level of granulosa cells in WT, *dnmt3aa*$^{-/-}$ and *dnmt3ab*$^{-/-}$ovaries at 120 dah. (**b**) Statistical analysis relative 5-mC staining level of WT, *dnmt3aa*$^{-/-}$ and *dnmt3ab*$^{-/-}$spermatogonia, spermatocytes and spermatozoa in testes at 120 dah. Results were presented as mean ± SD. Different letters above the error bar indicate statistical differences at $P < 0.05$ as determined by one-way ANOVA followed by Tukey's post-hoc test. SG, spermatogonia; SC, spermatocytes; SZ, spermatozoa. dah, day after hatching.

877 **Fig. S1**

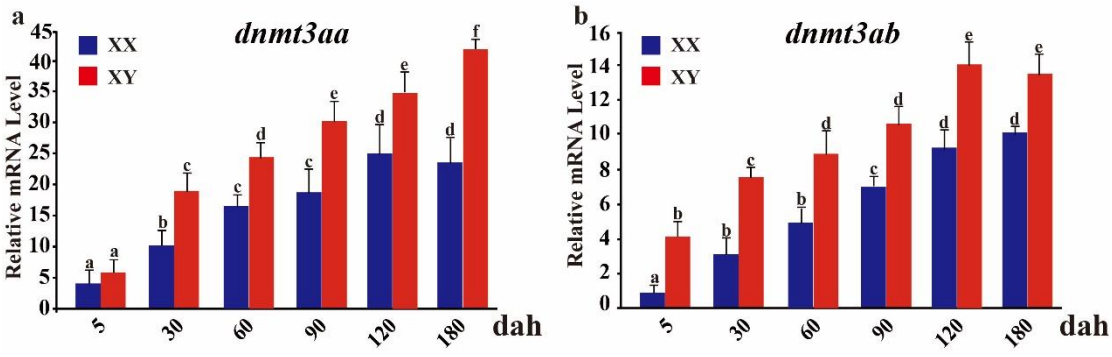

878

879

Fig. S2

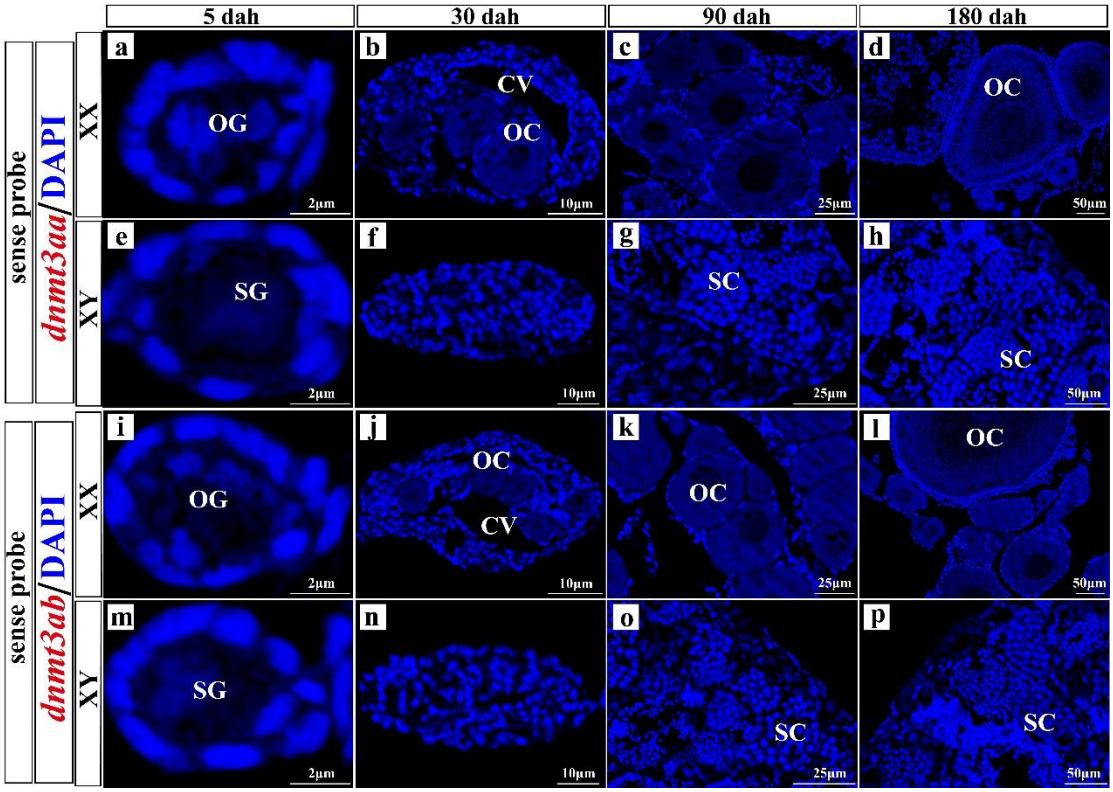
5 dah
30 dah
90 dah
180 dah
sense probe
dnmt3aa/DAPI
XX
XY
a
b
c
d
e
f
g
h
OG
CV
OC
SG
SC
2μm
10μm
25μm
50μm
sense probe
dnmt3ab/DAPI
XX
XY
i
j
k
l
m
n
o
p
OG
OC
CV
SG
SC
2μm
10μm
25μm
50μm

882 **Fig. S3**

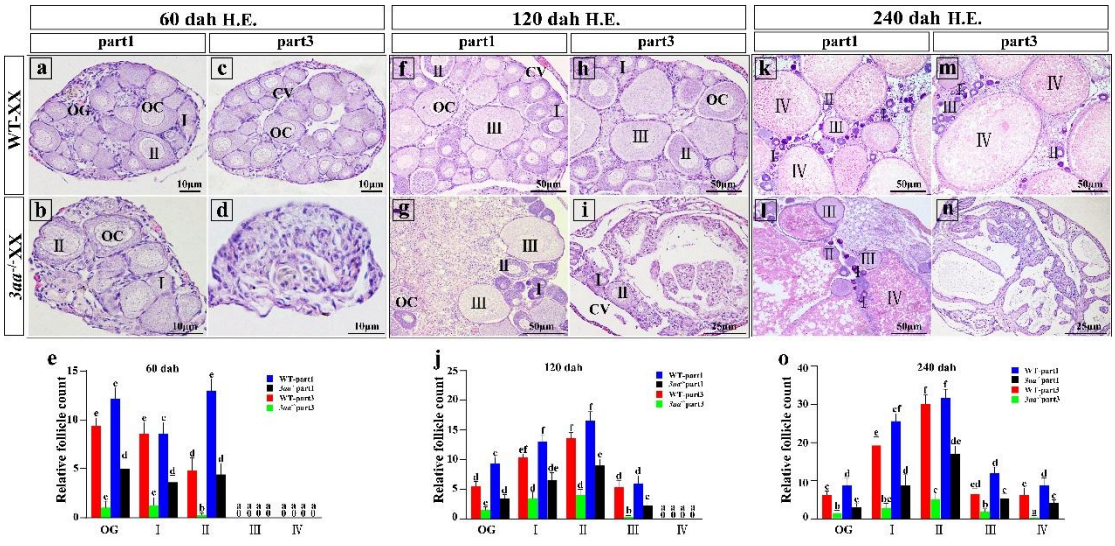

883

884

Fig. S4

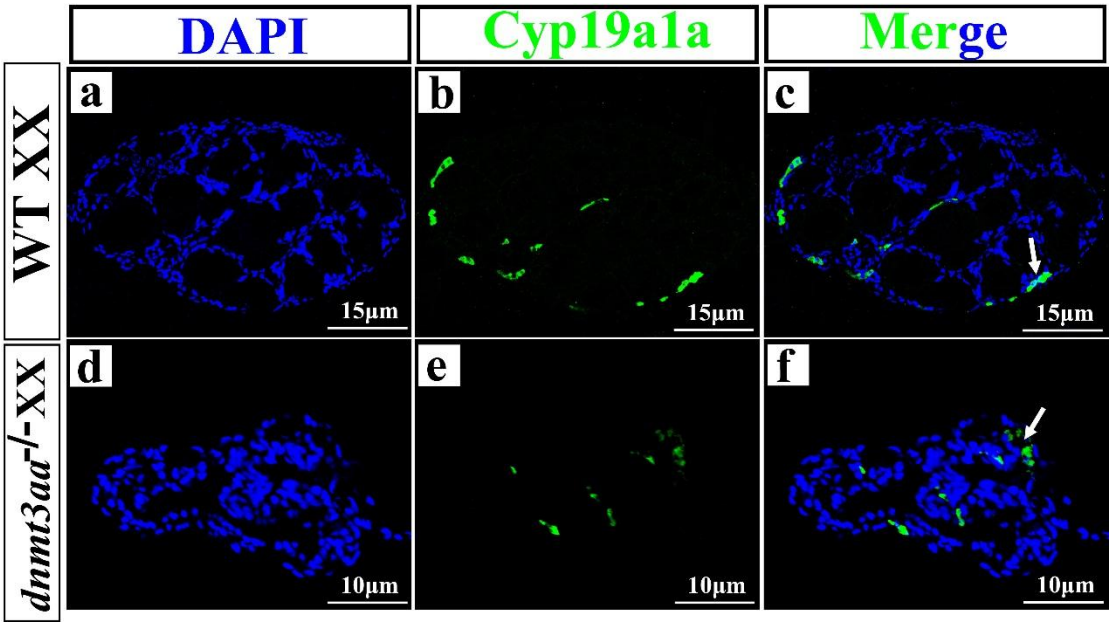
DAPI
Cyp19a1a
Merge
WT XX
dnmt3aa-/-XX
a
b
c
d
e
f
15μm
10μm

Fig. S5

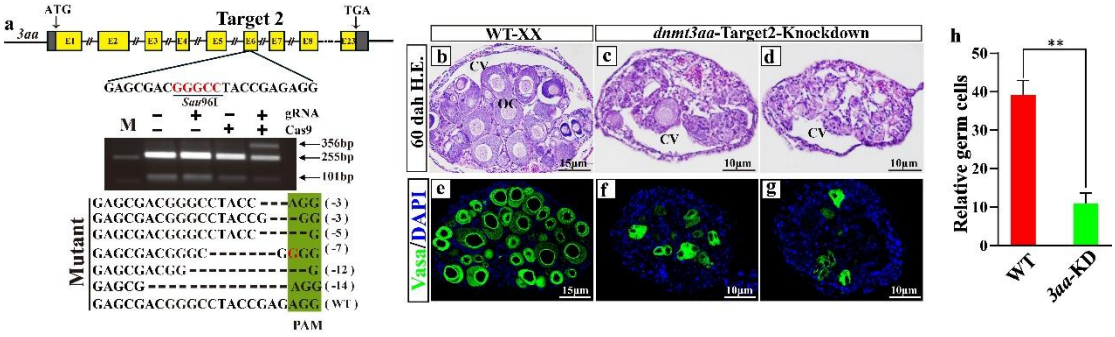
a
3aa
ATG
TGA
Target 2
GAGCGACGGGCCTACCGAGAGG
Sau96I
M
gRNA
Cas9
356bp
255bp
101bp
Mutant
GAGCGACGGGCCTACC---AGG (-3)
GAGCGACGGGCCTACCG---GG (-3)
GAGCGACGGGCCTACC-----G (-5)
GAGCGACGGGC-------GGG (-7)
GAGCGACGG----------G (-12)
GAGCG----------AGG (-14)
GAGCGACGGGCCTACCGAGAGG (WT)
PAM
WT-XX
dnmt3aa-Target2-Knockdown
60 dah H.E.
Vasa/DAPI
CV
OC
15μm
10μm
h
Relative germ cells
**
WT
3aa-KD

890 **Fig. S6**

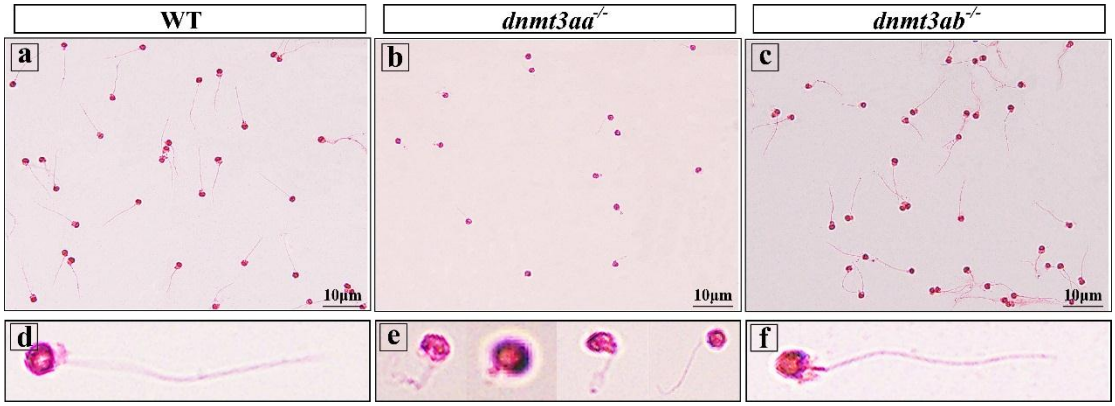

891

892 **Fig. S7**

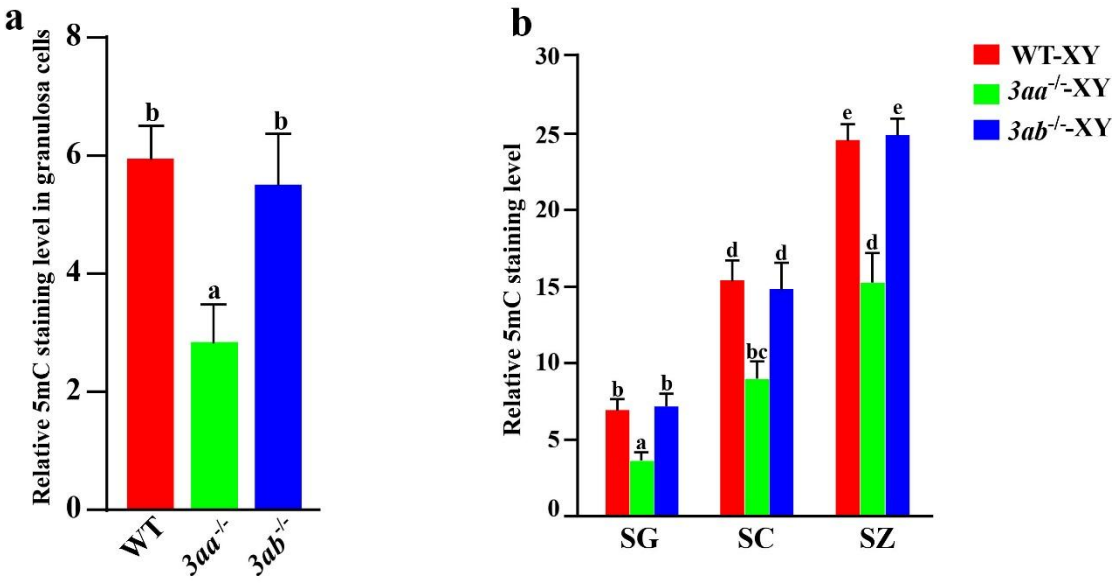

893

894

Additional file 2: Table S1. All primer sequences used in this study.

Primer name	Sequence (5'-3')	Purpose
gRNA-*dnmt3aa*-target 1-F	TAATACGACTCACTATAGGCAGACCA GGACAGTCCAGGTTTTAGAGCTAGAA	CRISPR/Cas9
gRNA-*dnmt3aa*-target 2-F	TAATACGACTCACTATAGGAGCGA CGGGCCTACCGAGGTTTTAGAGCTAGAA	
gRNA-*dnmt3ab*-target 1-F	TAATACGACTCACTATAGGAGAGAA CAATACTGGACTGTTTTAGAGCTAGAA	
gRNA-R	AGCACCGACTCGGTGCCAC	
dnmt3aa-KO-T1-detect-F	CCTGAAGAGCTTCTTAGCCACA	Mutant screening
dnmt3aa-KO-T1-detect-R	ATGCATGTTTAACAAACCTCTGC	
dnmt3ab-KO-detect-F	TGTCTCATTGTCCACTCAACCA	
dnmt3ab-KO-detect-R	TGTTGAATCAGACCTAATCACTGC	
dnmt3aa-KO-T2-detect-F	AACCTGCCAGCATGTACTCG	
dnmt3aa-KO-T2-detect-R	TGTTGTTGTGAAGGGGGAGG	
dnmt3aa-RT-PCR-F	CAGTCCAGAGGAGGGG	RT-PCR
dnmt3aa-RT-PCR-R	TCTCCCCTGGCGACTGGCTCGG	
dnmt3ab-RT-PCR-F	TGGACTCGGACCTGAT	
dnmt3ab-RT-PCR-R	CCTCCGCACGGCAAGAGGAAGG	
gapdh-F	AAGCTCATTTCCTGGTAT	
gapdh-R	CCTTTGCTGATTTCCTTG	
dnmt3aa-ISH-F	CCCAGACACCAGAGAACGAC	ISH
dnmt3aa-ISH-R	TGTTGTTGTGAAGGGGGAGG	
dnmt3ab-ISH-F	TCCACCAAAGCTTTACCCCC	
dnmt3ab-ISH-R	CCTGTTCATGCCAGGAAGGT	
dnmt1-qPCR-F	TGGCTCCCACGTTGATGAC	qRT-PCR
dnmt1-qPCR-R	AATTTGCCTTGCTCCTCCGT	
dnmt3aa-qPCR-F	TTGAGCCGGCCAAGTTGTAT	

dnmt3aa-qPCR-R	CATGCCGACAGTGATGGAGT	
dnmt3ab-qPCR-F	TCCACCAAAGCTTTACCCCC	
dnmt3ab-qPCR-R	CGGACGATACCCACAGTGAT	
dnmt3bb.1-qPCR-F	AATGAGAACAGCCCCCTGAC	
dnmt3bb.1-qPCR-R	CGCTCCTGAAGACTTGTCCG	
dnmt3ba-qPCR-F	CGAAAGAGGACGACAACCGT	
dnmt3ba-qPCR-R	GTTCATGCCAGGCAGGTTTC	
dnmt3bb.2-qPCR-F	CTTTACCTGAACCGGGCACA	
dnmt3bb.2-qPCR-R	TATTCCCTGGAACGCACAGG	
baxa-qPCR-F	TGCATCAGATTCACGATGAGTT	
baxa-qPCR-R	ACGAGTCGGCATGCAAAGTA	
baxb-qPCR-F	TGGCAATAAAGCAGTGACGA	
baxb-qPCR-R	CCTCTCTTGTGGGACAAAGT	
caspase3a-qPCR-F	GGAAAACAATCAGCGGGCTC	
caspase3a-qPCR-R	CGTCAGTACCGTTTCGCTGA	
caspase3b-qPCR-F	ACTGTGGCTCAGATGAAAAAGC	
caspase3b-qPCR-R	GACCCTTGCAGTGGTTTCCT	
caspase8-qPCR-F	CCGCAACAGCAGTTCACATT	
caspase8-qPCR-R	TCAGGAAGAGGGGTGGGATT	
caspase9-qPCR-F	TTCCTAGTAAGCTATCGCCTGA	
caspase9-qPCR-R	CTATGTTGGAGCCCTTGCGA	
AMH-F5	ATGGCTCCGAGACCTTGACTG	Genetic sex
AMH-R3	CAGAAATGTAGACGCCCAGGTAT	identification

896